Journal of Geoscience and Environment Protection, 2026, 14(9), 249-281
https://www.scirp.org/journal/gep
ISSN Online: 2327-4344
ISSN Print: 2327-4336

# Soil Quality and Potential Toxicity in Artisanal Mining Areas: Evidence from Obuasi-Adaase, Ghana

**Asare Asante-Annor[1*], Blessing Serwaa Duodu[1], Cindy Ankomah Gaisie[1], Albert Kafui Klu[1], Jamel Seidu[2]**

[1]Faculty of Geosciences and Environmental Studies, University of Mines and Technology, Tarkwa, Ghana
[2]School of Railway and Infrastructural Development, University of Mines and Technology, Essikado, Ghana
Email: *aasante-annor@umat.edu.gh

**How to cite this paper:** Asante-Annor, A., Duodu, B. S., Gaisie, C. A., Klu, A. K., & Seidu, J. (2026). Soil Quality and Potential Toxicity in Artisanal Mining Areas: Evidence from Obuasi-Adaase, Ghana. *Journal of Geoscience and Environment Protection, 14,* 249-281.
https://doi.org/10.4236/gep.2026.149014

**Received:** July 25, 2026
**Accepted:** September 25, 2026
**Published:** September 28, 2026





## Abstract

The contamination of soils is a problem that has recently become of major concern in the Ghanaian artisanal mining areas. Plants, humans, micro-organisms and other living species within the ecosystem that have a form of interaction with soils are highly at risk of the toxic element contamination within such areas. This study assessed the levels of Potentially Toxic Elements (PTEs) in soils around artisanal mining sites in the Adaase community in Obuasi, Ghana. Soil samples were picked from different locations around the mining sites. The concentrations of the various elements were analysed using geostatistical methods, pollution indices were used to determine the contamination levels, and their sources were traced using factor analysis. The parameters mainly employed include the Geo-accumulation Index (Igeo), the Enrichment Factor (EF), the Contamination Factor (CF), the potential ecological Risk Index (RI) and the Pollution Load Index (PLI) among others. The results showed that arsenic (As) is the major PTE in the area with a mean concentration of 80.90 ppm across the ten sampling locations, some six times the average shale background of 13 ppm. Arsenic returned a mean contamination factor of 6.22 (very high contamination), a mean geoaccumulation index of 1.89 (moderately polluted, rising to 2.98 at location D1) and a mean aluminium-normalised enrichment factor of 6.39 (significant enrichment), exceeding its threshold on all four indices at nine or ten of the ten locations. Other elements like manganese (Mn), chromium (Cr), nickel (Ni), copper (Cu), zinc (Zn), and lead (Pb) were found to be within permissible levels. These other elements have EF values, $0 \leq EF < 2$, indicating little enrichment, Igeo values, $-2 < Igeo < 1$, showing very low pollution and CF values, CF values below 1, showing low contamination throughout. The pollution load index remained below unity at every location, with a study-area value

of 0.599, indicating no overall deterioration in soil quality on that measure. The potential ecological risk index averaged 72.61 and ranged from 33.38 to 129.28, with arsenic accounting for between 72.2% and 91.4% of the risk at each location; because cadmium and mercury were not determined, this figure represents a lower bound. The findings point out the need for regular monitoring, soil remediation and sustainable mining practices to mitigate the risk posed by arsenic contamination and ensure environmental safety in the Adaase community.

## Keywords

Artisanal Mining, Soil Toxicity, Enrichment Factor, Contamination Factor, Arsenic, Obuasi

## 1. Introduction

Gold mining is a major economic contributor in Obuasi, Ghana, and it poses significant environmental issues, particularly in terms of soil pollution. One of the primary concerns is regarding the source of contamination of the soil with different elements such as arsenic (As), lead (Pb), cadmium (Cd), and mercury (Hg), which are harmful substances. Also known as Potentially Toxic Elements (PTEs), they are harmful metals that can persist in the environment for a long time and impact soil, water, and human health (Zhang et al., 2023b). They enter the soil through mining operations, such as digging up soil and rocks containing them, extracting gold using mercury, and disposing of mining waste improperly (Abdul-Wahab & Marikar, 2012). In artisanal gold mining, alluvial deposits are primarily mined along rivers, waterways and terrestrial soils (Donkor et al., 2006). Gold is known to occur with sulphide minerals like arsenopyrite and pyrite in the gold mining region of Obuasi. Artisanal mining is among the major sources of PTEs in Obuasi, leading to the leaching of the soil and water bodies. Some studies show that there is high contamination of PTEs near neglected mines and tailings dams (Bempah & Ewusi, 2016), but in artisanal mining areas, it can even be worse because the tailings are dumped with little or no care. Over time, these toxins slowly spread randomly in the soil, making it hard to know which areas will be affected next.

In Adaase, a farming community in Obuasi, artisanal mining, which poses a threat to soils, is becoming a serious problem. Farmers depend on the land for their crops, so the presence of PTEs in the soil will pose health and environmental threats to the people when they feed on plants that have absorbed PTEs. The toxic elements can also be breathed in by people or come in contact with their skin, posing serious health risks, especially to children.

Researchers have studied the various parameters of artisanal mining sites to evaluate the extent of contamination that mining activities have caused in the natural environment. Some of these concerns have resulted in studies involving hy-

drochemical analysis and geo-chemical modelling of groundwater and surface water bodies in artisanal mining communities (Ewusi et al., 2023). In other studies, such as Danala Danga et al. (2025), geo-chemical accumulation index was used to assess the contamination levels of artisanal mining sites in Cameroon and enriching factor to determine whether the PTEs are from a natural or anthropogenic origin. Kazapoe et al. (2022) used Principal Component Analysis (PCA) to analyse the relationship between toxic elements and the Geo-chemical accumulation Index (Igeo) to study the degree of PTEs pollution in soils around a mine tailing. Bartrem et al. (2014) found that soil contamination in mine sites can cause severe heavy metal contamination of water sources and poisoning of humans and animals, if ingested. Akoto et al. (2018) found high levels of arsenic, lead, and mercury in the soil around Obuasi, beyond safe limits for farming. Machine learning has also emerged as a tool for contamination studies. It has been used to identify high-risk contamination areas, as seen in studies conducted in Guangxi, China (Zhang et al., 2023a). Though it has proven to be a useful tool, it requires a large amount of data to work effectively. de Souza et al. (2017) concluded that artisanal mining contributes to PTE contamination in the environment.

In addition to the detection of PTEs, some studies have been conducted on the analytical methods and geostatistical modelling needed to adequately characterize soil contamination. In the last decade, researchers have been able to use more accessible analytical tools like X-Ray Fluorescence Spectroscopy (XRF), Inductively Coupled Plasma Mass Spectrometry (ICP-MS), and Atomic Absorption Spectroscopy (AAS) (Baveye et al., 2018; Rizvi et al., 2024). Darko et al. (2019) used XRF to assess the human health risks and bioaccessibility of toxic metals in the topsoils of a mining community in Ghana and found high concentrations of arsenic (As), chromium (Cr), nickel (Ni) and zinc (Zn) and suggested frequent monitoring of the accumulation of metals in the topsoil. To vividly describe how PTEs are distributed across a site, geostatistical approaches such as ordinary kriging, empirical Bayesian kriging, and inverse distance weighting are increasingly combined with GIS to interpolate PTE concentrations from limited sampling points (Xiao et al., 2020; Selahvarzi et al., 2023).

Alongside these techniques, pollution indices provide standardised ways of quantifying contamination severity. The Geo-accumulation Index (Igeo), Contamination Factor (CF), and Pollution Load Index (PLI) are among the most widely applied, with Jahan et al. (2024) reporting moderate to high CF values for arsenic, cobalt, chromium, copper, lead, and zinc, and Gololobova and Legostaeva (2023) showing how the PLI combines data from multiple elements into a single overall measure of soil quality. GIS-based spatial mapping has similarly been used to visualise contamination patterns at a landscape scale. For instance, Xiao et al. (2020) mapped the distribution of five PTEs across more than a thousand soil samples in Xiangzhou, China, while Luo et al. (2021) used GIS to trace PTE contamination in rainwater runoff from a manganese mining area in Xiangtan, China, in support of a health risk assessment.

Assessing soil pollution is crucial to protect the soil's role in the environment and ensure it remains suitable for farming. However, it has been found from literature that research works undertaken in this regard within the Obuasi area, including Adaase, mostly focus on water assessment and not on soils (Adomako & Ampadu, 2015). Hence, this study is aimed at assessing the levels of Potentially Toxic Elements (PTEs) in soils at artisanal mining sites in the Obuasi area; identifying hotspots of PTE concentration within the study area; and apportioning the identified toxic elements to their respective sources.

## 2. Study Area

### 2.1. Location

The Adaase community is found in the northern part of the Obuasi Municipality. Obuasi is in the Ashanti region of Ghana, it is located at latitude 6˚12'00" north, longitude 1˚40'00" west. The Obuasi municipality can be accessed by paved roads from Accra, Accra-Takoradi and the Yamoranza-Asante-Bekwai inland roads. The location and accessibility of the study area are shown in Figure 1.

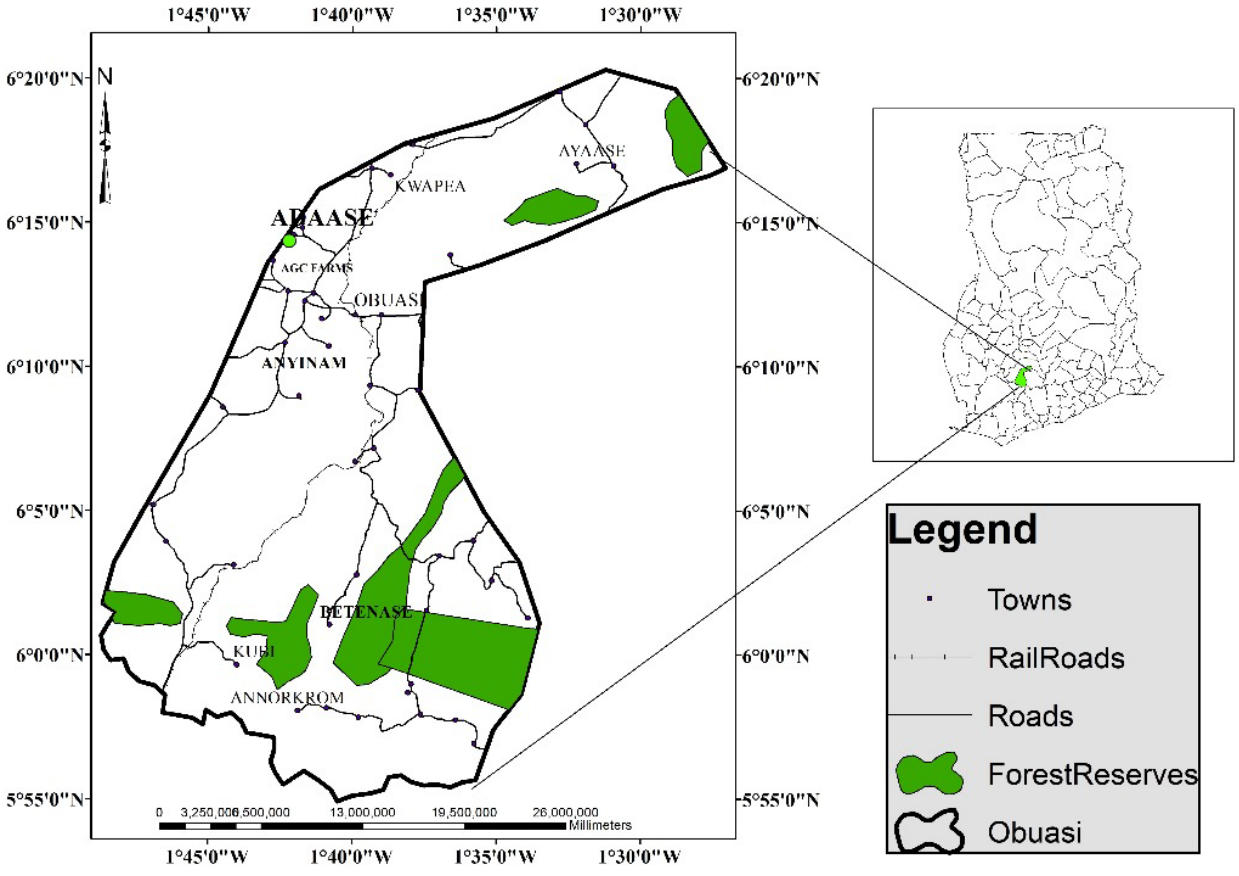


Figure 1. Location and accessibility map of the study area.

The climate of Obuasi is classified as a tropical wet and dry climate under the Köppen-Geiger system. This type of climate is warm throughout the year, with an

average annual temperature of 25.5˚C. Obuasi receives 1259 mm to 1750 mm of rainfall yearly, and the humidity is usually high, averaging 75% to 80% during the rainy seasons (Anarfi et al., 2020). These weather conditions are good for farming but can also cause problems like flooding when there are heavy rains and water shortages during dry seasons (Bempah & Ewusi, 2016). In the past, the area was covered by thick tropical rainforest, but mining has caused a lot of deforestation and land degradation. Measures are being put in place to restore the vegetation. However, potentially toxic elements have been released into the soil through mining, which makes it harder for plants to grow. These metals can accumulate in crops and disturb human health. This stays a big challenge for farming and vegetation in the area (Darko Asamoah et al., 2024; Bempah & Ewusi, 2016). Regardless of these challenges, the vegetation in Obuasi is still essential for keeping the environment balanced, supporting farming and reducing the effects of climate change (Adu-Poku et al., 2012). Vegetation in the area stays critical for maintaining ecological balance, supporting livelihoods, and mitigating the impacts of climate change.

## 2.2. Geology

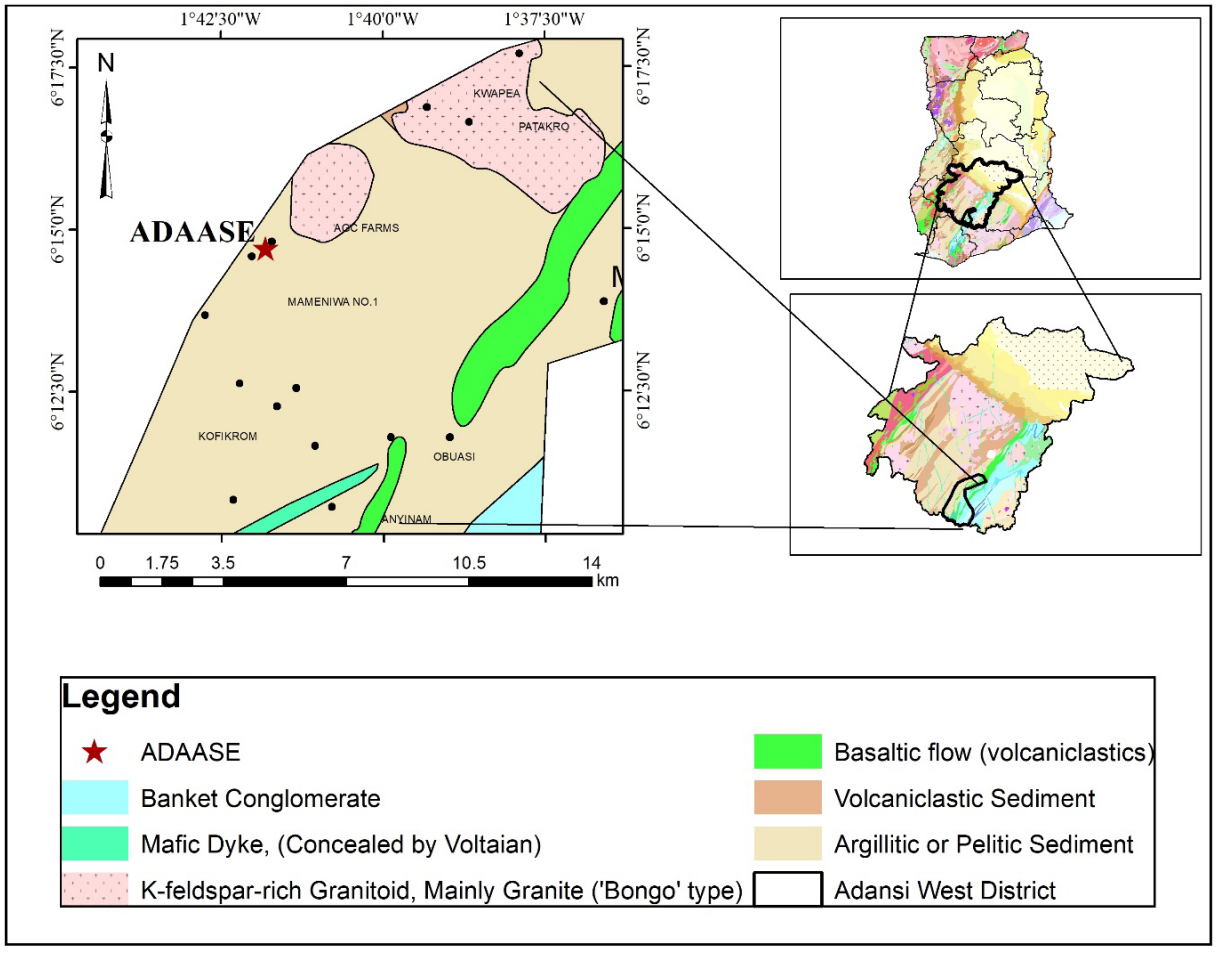


**Figure 2.** Geological map of the study area.

The geology of Obuasi and its geological features, as shown in **Figure 2**, is shaped by natural processes that led to one of the richest gold deposits' formations, globally. The area belongs to the Birimian Supergroup, a large rock formation in West Africa known for its gold deposits. These rocks were formed about 2.1 - 2.2 billion years ago and they include phyllites, greywackes, volcanic rocks and gold-bearing granites (Sunkari et al., 2024).

One most important characteristic of the area is the Obuasi Shear Zone. A large crack in the Earth's crust that acted like a pathway for these gold-rich fluids. These fluids, which were hot and carried dissolved gold, were transported through the cracks and interacted with the surrounding rocks. As the fluids cooled, the gold settled in the rocks, majority of them in quartz veins and areas rich in sulphide minerals such as arsenopyrite and pyrite (Oberthür et al., 1997; Oliver et al., 2020). The host rocks, mainly greywackes and phyllites, were originally sediments deposited by rivers and weathering of older rocks. Over time, these sediments were buried, squeezed and turned into harder rocks. The area is full of intersecting faults, folds, and cracks, which created a system for the fluids to flow through. Over time, as tectonic forces continued to act, these cracks became more open, allowing the fluids to flow and deposit gold in multiple stages (Odling, 2022).

## 3. Materials and Methods

### 3.1. Field Visit and Soil Sampling

The field visit was a key part of this research, allowing direct observation and data collection from the study areas. The visit included an artisanal mining site, a nearby farm, a school, and residential areas to collect soil samples for analysis. A total of 10 topsoil samples were collected from five (5) locations around the artisanal mining sites at a depth of 50 cm using a spade. These locations include two separate abandoned mining sites, a farm nearby, a school and a residence. Other details of the sampling sites can be found in **Figure 3** and **Table 1**. These sites were chosen for sample collection to ascertain the level of degradation of the land in the community. Food crops from farms and homes would have to be guaranteed of a good level of quality for the inhabitants. To prevent contamination of the samples during transport, the samples were stored in sealed airtight bags and transported to the lab for further analysis.

**Table 1.** Locations for sample collection.

| ID | Location | Easting | Northing | Distance from Pit (m) |
|---|---|---|---|---|
| A | Site 1 | 643,758 | 690,775 | 0 |
| B | Site 2 | 644,260 | 690,594 | 0 |
| C | Farm | 643,656 | 690,945 | 100 |
| D | School | 643,843 | 690,437 | 300 |
| E | Residence | 643,741 | 690,478 | 300 |


Figure 3. Locations for sample collection in Obuasi-Adaase community.

## 3.2. Sample Preparation and Laboratory Analysis

Ten samples were collected from the sampling locations in study area and analysed separately, three duplicates per location were analyzed at the Ghana Geological Survey Authority Laboratory in Accra in May 2025. The values reported throughout this paper are the means of the three subsamples at each location, and n = 10 accordingly refers to location means rather than to individual analyses. Soil samples were air-dried, sieved to ensure homogeneity, and split into two portions for pH determination and X-Ray Fluorescence (XRF) analysis, conducted at the Environmental Laboratory in the University of Mines and Technology, Ghana and the Ghana Geological Survey Authority, respectively.

For XRF analysis, samples were oven-dried for 24 hours and sieved to 90 μm. A 4.0 g aliquot of each sample was homogenised with 0.9 g of Hoechst wax binder and pressed into a 32 mm pellet under 15 tons of pressure using a hydraulic press. Multi-element composition was determined using an energy-dispersive polarising XRF spectrometer (Olympus Vanta M Series, 50 kV, 0.2 mA). To minimise contamination, gloves were worn throughout sample handling, mixing equipment was cleaned with acetone between samples, and pellet surfaces were not touched prior to analysis.

For pH determination, 30 g of soil was mixed with 150 mL of deionised water in a 1:5 soil-to-water ratio, shaken for 45 min on an orbital shaker, and allowed to settle for approximately 3 hours. Soil pH was then measured using a calibrated pH meter, with readings recorded once stable.

## 3.3. Statistical Analysis

### 3.3.1. Descriptive Statistics

Descriptive statistics, including mean, median, minimum, maximum, range, variance, standard deviation, skewness, and kurtosis, were computed to characterise the distribution and variability of each soil property (Akoto et al., 2018).

Standard deviation was used to assess data dispersion about the mean, while skewness described deviation from a normal distribution -positive values indicating a right-skewed distribution, negative values indicating a left-skewed distribution, and values near zero indicating symmetry (Khalili et al., 2020; Mahvi et al., 2022).

#### 3.3.2. Multivariate Statistical Analysis

Of the 21 elements determined by XRF, nine were retained for multivariate analysis: eight potentially toxic elements (Cr, Mn, Fe, Ni, Cu, Zn, As and Pb) together with Al, which was included as a conservative lithogenic reference element to help distinguish geogenic from anthropogenic associations. Restricting the variable set in this way also limited the number of variables relative to the ten available cases. A two-tailed Spearman's correlation matrix was used to assess relationships among the retained elements. R-mode Factor Analysis (FA), using Principal Component Analysis (PCA) with varimax rotation, was applied to identify groupings of related variables. Sampling adequacy was assessed using the Kaiser-Meyer-Olkin (KMO) measure and Bartlett's test of sphericity. The KMO value was 0.470, below the 0.50 minimum generally regarded as acceptable for factor analysis (Kaiser, 1974), while Bartlett's test was significant (chi-square = 83.550, df = 36, $p < 0.001$), confirming that the correlation matrix differed from an identity matrix. The factor solution is accordingly reported as exploratory. Factor analysis was used to infer whether soil contamination originated from anthropogenic or natural sources; only factors with eigenvalues greater than one were retained, yielding five principal factors (Sunkari et al., 2019). Hierarchical Cluster Analysis (HCA), presented as a dendrogram, was performed to further examine inter-elemental relationships and validate the factor analysis results. All statistical analyses were conducted using SPSS version 27.

### 3.4. PTEs Pollution Assessment

The pollution status and environmental risk of Potentially Toxic Elements (PTEs) in soils were evaluated using the Enrichment Factor (EF), Geo-accumulation Index (Igeo), Contamination Factor (CF), and Pollution Load Index (PLI). No published pristine pre-mining background dataset exists for Obuasi covering the elements in the study area, so a global lithological reference is used throughout for internal consistency. Average shale after Turekian and Wedepohl (1961) is the most widely used background reference for Igeo, CF, EF and PLI in the soil and sediment pollution literature and has been applied in the Obuasi area (Darko Asamoah et al., 2024; Akoto et al., 2018). All the 21 elements used in the estimation of the various PTEs used background values from Turekian and Wedepohl (1961), average shale.

#### 3.4.1. Enrichment Factor

The Enrichment Factor (EF) was used to normalise and assess metal concentrations relative to a conservative reference element using Equation (1) (Ackerman et al., 1980; Fosu-Mensah et al., 2018; Sutherland, 2000).

$$EF = (M/AI)\ \text{sample} / (M/AI)\ \text{background} \quad (1)$$

where (M/Al) sample is the metal to Al ratio in the sample, and (M/Al) background is the corresponding background ratio. Aluminium was adopted as the conservative reference element in preference to iron. Iron is not conservative in this dataset: it has a coefficient of variation of 58.8% against 21.1% for aluminium, and it loads 0.93 on the first principal component alongside Cu and Ni while pairing most closely with Cu in the cluster analysis, indicating that it forms part of the enriched metal association rather than an inert lithogenic reference. The choice is supported by agreement with the other indices: across the ten locations, the aluminium-normalised EF for arsenic tracks its contamination factor at r = 0.933 and its geoaccumulation index at r = 0.883, whereas the iron-normalised EF tracks the same two indices at only r = 0.334 and r = 0.170. EF values were interpreted using the five-tier classification of Sutherland (2000) and Fosu-Mensah et al. (2018), as shown in **Table 2**.

**Table 2.** Enrichment factor classes (Sutherland, 2000; Fosu-Mensah et al., 2018).

| Enrichment Factor (EF) | Enrichment Classes |
|---|---|
| EF < 2 | Little Enrichment |
| 2 ≤ EF ≤ 5 | Moderate Enrichment |
| 5 < EF < 20 | Considerable Enrichment |
| 20 < EF < 40 | Strong Enrichment |
| EF ≥ 40 | Extreme Enrichment |

### 3.4.2. GEO-Accumulation Index (Igeo)

The Geo-chemical Index (Igeo) was introduced by Müller (1969) as a method to identify and assess metal contamination in soils by comparing current PTEs concentrations to pre-industrial levels. The Igeo is calculated using Equation (2).

$$\text{Igeo} = \log_2\left[\frac{\text{Cn}}{1.5\text{Bn}}\right] \quad (2)$$

where Bn is the background value of the metal, taken as the average shale composition of Turekian and Wedepohl (1961) and applied uniformly to all 21 elements, Cn is the metal n's measured concentration in the soil, and factor 1.5 is applied to correct for lithological variations in the background data. Igeo was computed separately for each element at each of the ten sample locations, and the values reported are the mean, minimum, maximum and standard deviation of those per-location indices. Because the logarithm is non-linear, the mean of the per-location indices differs slightly from the index computed from the pooled mean concentration, and the per-location convention is applied throughout so that the reported ranges and the count of locations exceeding Igeo zero refer to the same quantity. The Igeo values are divided into seven categories: Class 0 (Igeo ≤ 0) indicates that the area is practically unpolluted. Class 1 (0 < Igeo < 1) represents areas that are unpolluted to moderately polluted. Class 2 (1 < Igeo < 2) indicates moderately polluted. Class

3 (2 < Igeo < 3) indicates moderate to strongly polluted areas. Class 4 (3 < Igeo < 4) indicates strongly polluted. Class 5 (4 < Igeo ≤ 5) indicates strong to very strongly polluted, and Class 6 (Igeo > 5) signifies severe pollution (Gupta et al., 2014; Müller, 1969), as shown in **Table 3**.

**Table 3.** Geo-accumulation index classes (Gupta et al., 2014; Müller, 1969).

| Geo-accumulation Index (Igeo) | Description | Pollution Classes |
|---|---|---|
| Igeo ≤ 0 | Unpolluted | Class 0 |
| 0 < Igeo < 1 | Unpolluted to Moderately Polluted | Class 1 |
| 1 < Igeo < 2 | Moderately Polluted | Class 2 |
| 2 < Igeo < 3 | Moderate to Strongly Polluted | Class 3 |
| 3 < Igeo < 4 | Strongly Polluted areas. | Class 4 |
| 4 < Igeo ≤ 5 | Strong to Severely Polluted | Class 5 |
| Igeo > 5 | Severely Polluted | Class 6 |

### 3.4.3. Contamination Factor (CF)

The Contamination Factor (CF) is calculated as the ratio of the concentration of a specific metal in sediments to its background value, as in Equation (3) (Fosu-Mensah et al., 2018; Hakanson, 1980).

$$\mathrm{CF} = \frac{C_{\text{sample}}}{C_{\text{background}}} \tag{3}$$

The Contamination Factor (CF) levels were interpreted as follows: CF < 1 indicates no or low contamination, 1 ≤ CF < 3 represents moderate contamination, 3 ≤ CF < 6 indicates strong contamination, and CF ≥ 6 signifies very strong contamination (Fosu-Mensah et al., 2018; Hakanson, 1980), as shown in **Table 4**.

**Table 4.** Contamination factor pollution classes (Fosu-Mensah et al., 2018; Hakanson, 1980).

| Contamination Factor (CF) | Pollution Classes |
|---|---|
| CF < 1 | Low Contamination |
| 1 ≤ CF < 3 | Moderate Contamination |
| 3 ≤ CF < 6 | Strong Contamination |
| CF ≥ 6 | Very Strong Contamination |

### 3.4.4. Pollution Load Index (PLI)

The Pollution Load Index (PLI) was calculated using the CFs in Equation (3) as shown in Equation (4) (Tomlinson et al., 1980).

$$\mathrm{PLI} = \frac{\sqrt{(\mathrm{CF1} \times \mathrm{CF2} \times \mathrm{CF3} \times \cdots \mathrm{CF}n)1}}{n} \tag{4}$$

The numerical values in the above equation provide a simple framework for estimating the level of PTE contamination in the soils. A PLI value greater than 1

(PLI > 1) indicates the presence of PTE contamination while a PLI value less than 1 (PLI < 1) shows that there is no contamination, as shown in Table 5.

Table 5. Pollution load index description and classes (Benarabi et al., 2021; Tomlinson et al., 1980).

| Pollution Load Index (PLI) | Description | Pollution Classes |
|---|---|---|
| PLI < 1.5 | Clean/Very Low Pollution | Class 1 |
| 1.5 ≤ PLI < 2 | Low Pollution | Class 2 |
| 2 ≤ PLI < 4 | Moderate Pollution | Class 3 |
| 4 ≤ PLI < 8 | Significant Pollution | Class 4 |
| 8 ≤ PLI < 16 | Very High Pollution | Class 5 |
| 16 ≤ PLI < 32 | Extremely High Pollution | Class 6 |
| PLI ≥ 32 | Excessive Pollution | Class 7 |

### 3.5. Potential Ecological Risk Index (RI)

The Potential Ecological Risk Index method was developed by Swedish scientist Hakanson in 1980 and it is widely used to evaluate the harmful effects of heavy metals in sediments and assess their potential ecological risks (Hakanson, 1980). The RI method is used to assess the potential for ecological harm from contaminants, particularly heavy metals, in soil and sediments. It considers both the concentration of the contaminant and its toxicity (Liu et al., 2021). The RI was calculated using Equation (5) (Hakanson, 1980).

$$\mathrm{RI} = \sum \mathrm{Eri} = \sum \left( \mathrm{Tri} \times \mathrm{CF}_i \right) \tag{5}$$

where Eri is the potential ecological risk factor of an individual element *i*, Tri is the toxic response factor of element *i*, and $\mathrm{CF}_i$ is the contamination factor of element i obtained from Equation (3).

An RI < 150 indicates low-grade ecological risk. 150 ≤ RI < 300 indicates moderate ecological risk. 300 ≤ RI < 600 indicates severe ecological risk, and an RI > 600 indicates serious ecological risk, as shown in Table 6.

Table 6. Scope of RI and general level of RI (Hakanson, 1980; Hamid et al., 2022).

| Scope of RI | General Level of RI |
|---|---|
| RI < 150 | Low-grade |
| 150 ≤ RI < 300 | Moderate |
| 300 ≤ RI < 600 | Severe |
| RI ≥ 600 | Serious |

### 3.6. Quality Assurance and Quality Control

Elemental analysis of soil samples was performed using a handheld Olympus Vanta VMR X-Ray Fluorescence (XRF) analyser (serial No. 803781, GeoChem mode,

40 kV, graphene detector window) at the Ghana Geological Survey Authority Laboratory, following field-portable XRF protocols for soil and sediment analysis (USEPA, 2007; Kalnicky & Singhvi, 2001). The analyser was factory-calibrated using fundamental parameters calibration and periodically verified against Certified Reference Material NIST SRM 2711a (Montana II Soil; NIST, 2009), consistent with recommended handheld-XRF QA/QC practice (USEPA, 2007). Instrument detection limits (3σ, 99.7% confidence, silica-blank basis) for the elements of principal interest were: As 1 mg/kg, Pb 2 mg/kg, Zn 1 mg/kg, Cu 2 mg/kg, Cr 8 mg/kg, Ni 4 mg/kg, Mn 5 mg/kg, and Fe 12 mg/kg (Olympus Corporation, n.d.). Concentrations below the respective LOD were recorded as non-detects.

**Table 7.** Analytical precision for selected elements from triplicate XRF analysis of soil samples.

| Element | Mean RSD (%) | Range (%) |
|---|---|---|
| Al | 0.7 | 0.4 - 1.2 |
| Fe | 0.2 | 0.0 - 0.5 |
| As | 1.6 | 0.9 - 2.5 |
| Zn | 6.4 | 2.0 - 12.6 |
| Cu | 7.2 | 3.0 - 12.5 |
| Mn | 10.9 | 3.8 - 30.8 |
| Ni | 11.8 | 6.2 - 21.5 |
| Pb | 13.2 | 4.9 - 27.3 |
| Cr | 18.9 | 2.6 - 92.4 |

Ten samples (A1, A2, B1, B2, C1, C2, D1, D2, E1, E2) were each analysed in triplicate, and precision was expressed as Relative Standard Deviation (RSD) in Table 7. Major elements (Al, Fe) showed excellent reproducibility (RSD < 1%), and As, Zn, and Cu showed good precision (mean RSD < 10%). Occasional elevated RSD for Mn, Pb, and Cr (notably one Cr replicate at sample B1) reflects proximity to instrument detection limits rather than sample heterogeneity, a recognised limitation of field-portable XRF near the LOD (Kalnicky & Singhvi, 2001).

### 3.7. Limitations of Methods

The multivariate statistical analyses (PCA and HCA) were conducted on a limited sample size (n = 10) relative to the number of variables analysed (nine elements), which is below conventional recommendations for factor analysis (typically a minimum 5:1 case-to-variable ratio). The sampling-adequacy diagnostics reflect this constraint: the Kaiser-Meyer-Olkin measure was 0.470, below the 0.50 minimum generally regarded as acceptable, although Bartlett's test of sphericity was significant (chi-square = 83.550, df = 36, $p < 0.001$), indicating that the correlation matrix was factorable in principle and that the binding limitation is the number of

cases rather than an absence of inter-elemental correlation. Consequently, the factor structure and inferred source groupings should be interpreted strictly as exploratory and hypothesis-generating rather than statistically confirmatory, and individual factor loadings should not be treated as stable estimates. It is noted, however, that the element groupings recovered by the Spearman correlation matrix, the factor analysis and the hierarchical cluster analysis were mutually concordant, which lends confidence to the broad source associations inferred, even though the number of factors retained, the variance explained and the individual loadings remain provisional. Because all three procedures derive from the same correlation matrix, this concordance reflects internal consistency rather than independent replication. Future studies should expand the sample size to improve the robustness and generalisability of the multivariate results.

A further limitation applies to the pollution indices. The geoaccumulation index, contamination factor, enrichment factor, pollution load index and potential ecological risk index are all computed against the same set of background values, so a change in the reference set propagates to every classification reported. The sensitivity is greatest for arsenic, whose mean geoaccumulation index of 1.89 lies close to the boundary between Müller classes 2 and 3, such that a modest revision of the arsenic background value would alter its reported class. The value adopted, 13 ppm, has been verified against the primary source, so the residual sensitivity lies in the choice of reference composition rather than in the accuracy of the figure taken from it. Classifications should therefore be read as relative to the reference composition adopted in Section 3.3 rather than as absolute statements of contamination.

## 4. Results and Discussion

### 4.1. Field Observations

During the field visit to artisanal mining sites in the Adaase community, several observations relevant to potential PTE contamination were made. Farms were observed near the mining sites, raising concerns about the potential contamination of agricultural soils with Potentially Toxic Elements (PTEs). This proximity increases the likelihood of crop uptake of harmful metals, posing potential health risks to the local population through dietary exposure. Interaction with a local resident also revealed that gold extraction is not conducted on-site, a deliberate measure by miners to prevent robbery, meaning mercury is not used at the site, thereby reducing the likelihood of mercury contamination in the immediate environment.

### 4.2. Geo-Chemical Analysis

Table 8 displays the concentrations and statistical summaries of elements in soil samples collected from around mining sites in the study area (Adaase). The mean concentrations (ppm) of the potentially toxic elements decrease in the following order: Fe > Mn > Cr > As > Zn > Cu > Ni > Pb. Pb and Ni recorded the lowest mean values, whereas Fe and Mn recorded the highest. Mean concentrations of Mn,

Cr, As, Zn, Cu, Ni and Pb were compared against the Canadian Council of Ministers of the Environment (CCME, 2007) agricultural soil quality guidelines, only arsenic and chromium exceeded these thresholds. Arsenic (80.90 ppm) exceeded the CCME limit of 12 ppm by a factor of ~6.7. Chromium (83.03 ppm) exceeded the CCME guideline of 64 ppm by a factor of 1.3. Manganese (123.20 ppm), zinc (37.13 ppm), copper (26.33 ppm), nickel (21.90 ppm) and lead (13.87 ppm) all fell below their respective guidelines, with nickel and lead more than threefold under. Soils around the Adaase mining sites are therefore contaminated with respect to arsenic, and marginally so with respect to chromium under the more conservative CCME criterion; the remaining elements pose no guideline-based concern. Guideline exceedance and geochemical enrichment are treated as distinct here, the pollution indices reported below are calculated against the average shale composition of Turekian and Wedepohl (1961) and thus reflect enrichment relative to crustal background rather than breach of a health- or ecology-based threshold.

The pH of the soil ranged from 4.80 to 6.96 with a mean value of 5.80. This indicates that the soil is generally acidic in this area. The acidic nature of the soil may increase the mobility and toxicity of PTEs, posing potential risks to plants and organisms. All eight potentially toxic elements, ranging from 0.03 for Cr to 1.86 for Zn, have positive skewness, indicating that for these parameters, most of the values are concentrated on the lower side of the range, with a few higher values pulling the tail to the right. The effect is most pronounced for Zn (1.86) and Mn (1.25), which also record the highest kurtosis values (3.26 and 1.70 respectively), reflecting a small number of markedly enriched samples. Aluminium, by contrast, is negatively skewed (−0.41), consistent with its behaviour as a lithogenic reference element rather than a contaminant.

**Table 8.** Descriptive statistics of elemental concentrations in soil samples.

| Element | N | Minimum | Maximum | Mean | Median | SD | CV (%) | Skewness | Kurtosis |
|---|---|---|---|---|---|---|---|---|---|
| Al/ppm | 10 | 59861.00 | 108103.67 | 86313.90 | 90524.17 | 18248.97 | 21.14 | −0.41 | −1.51 |
| Si/ppm | 10 | 252206.33 | 302586.33 | 281589.50 | 289202.00 | 19212.63 | 6.82 | −0.46 | −1.68 |
| K/ppm | 10 | 5257.67 | 12942.00 | 8373.50 | 7996.50 | 2734.10 | 32.65 | 0.58 | −1.01 |
| Ti/ppm | 10 | 5307.33 | 7792.67 | 6693.80 | 6932.00 | 1105.69 | 16.52 | −0.21 | −2.17 |
| V/ppm | 10 | 44.67 | 71.00 | 56.93 | 56.83 | 7.22 | 12.67 | 0.32 | 0.87 |
| Cr/ppm | 10 | 45.00 | 121.00 | 83.03 | 80.33 | 21.62 | 26.04 | 0.03 | 0.15 |
| Mn/ppm | 10 | 35.00 | 316.67 | 123.20 | 112.67 | 86.95 | 70.58 | 1.25 | 1.70 |
| Fe/ppm | 10 | 12626.67 | 69917.33 | 37044.77 | 33828.00 | 21782.67 | 58.80 | 0.49 | −1.22 |
| Ni/ppm | 10 | 16.00 | 29.00 | 21.90 | 22.00 | 3.63 | 16.60 | 0.29 | 0.87 |
| Cu/ppm | 10 | 18.67 | 36.33 | 26.33 | 25.33 | 6.86 | 26.06 | 0.34 | −1.59 |
| Zn/ppm | 10 | 22.33 | 86.00 | 37.13 | 27.50 | 20.37 | 54.86 | 1.86 | 3.26 |
| As/ppm | 10 | 31.33 | 153.67 | 80.90 | 78.83 | 39.07 | 48.29 | 0.47 | −0.51 |
| Rb/ppm | 10 | 42.00 | 83.00 | 59.10 | 58.00 | 15.20 | 25.72 | 0.23 | −1.72 |

**Continued**

| | | | | | | | | |
|---|---|---|---|---|---|---|---|---|
| Sr/ppm | 10 | 49.00 | 138.00 | 83.93 | 75.33 | 31.38 | 37.39 | 0.82 | −0.48 |
| Y/ppm | 10 | 22.67 | 42.67 | 30.80 | 30.00 | 6.37 | 20.69 | 0.51 | −0.28 |
| Zr/ppm | 10 | 219.33 | 416.67 | 307.80 | 291.67 | 66.66 | 21.66 | 0.54 | −0.58 |
| Nb/ppm | 10 | 15.67 | 23.67 | 20.13 | 20.33 | 2.57 | 12.76 | −0.38 | −0.80 |
| Mo/ppm | 10 | 2.00 | 9.33 | 6.17 | 6.00 | 2.23 | 36.15 | −0.33 | 0.03 |
| Pb/ppm | 10 | 9.67 | 19.00 | 13.87 | 13.83 | 3.00 | 21.63 | 0.32 | −0.84 |
| Th/ppm | 10 | 0.00 | 13.67 | 9.17 | 10.67 | 4.25 | 46.42 | −1.16 | 1.10 |
| U/ppm | 10 | 0.00 | 2.67 | 0.67 | 0.00 | 0.94 | 141.42 | 1.18 | 0.57 |

### 4.3. Box and Whisker Analysis

Box and whisker plots of all 21 elements determined by XRF are presented in Figure 4 to visualise the distribution of elemental concentrations in the soil samples collected. Concentrations are plotted on a logarithmic axis in ppm to accommodate the five orders of magnitude spanned by the data set, from below 1 ppm for U to approximately 280,000 ppm for Si. On this scale, the height of each box represents proportional rather than absolute variability, so boxes may be compared directly across elements of very different abundance. This was done to assess data spread, identify outliers, compare data depths and assess soil contamination (Sunkari et al., 2019).

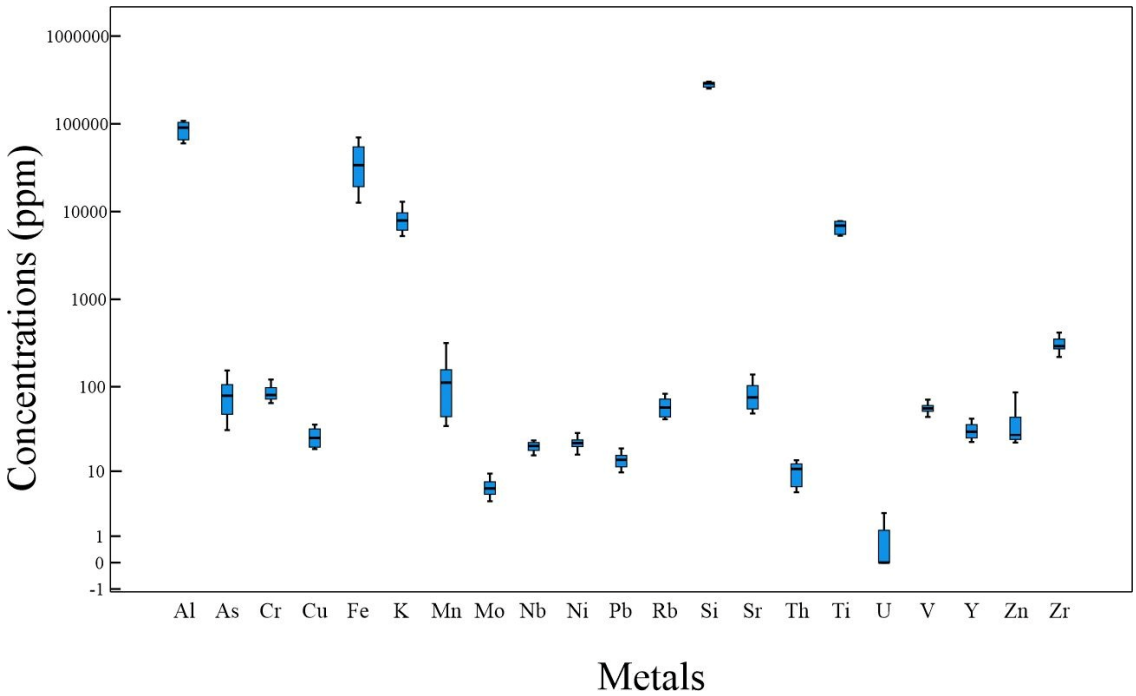


Figure 4. Box and Whisker plots of the elements in the study area, concentrations in ppm on a logarithmic scale (dash lines in the boxes are the means whereas the solid lines represent the median).

The boxplots for Ni, Pb, Cr and Cu show that the data are tightly grouped with

small ranges, their coefficients of variation being 16.6%, 21.6%, 26.0% and 26.1% respectively. The middle values (medians) are close to the centre of the boxes, which means the data is evenly spread on both sides. The whiskers extend to the minimum and maximum observed values rather than to a fitted outlier threshold, and for these elements, they are short, indicating that the data do not vary much between samples. The similar levels of these elements in all the samples suggest they are naturally present in the environment, with no signs of pollution or unusual increases in their amounts (Borges, 2023). The major matrix elements Si, Al, Ti and V likewise plot as narrow boxes, Si being the least variable element in the data set at a coefficient of variation of 6.8%, which is consistent with a uniform lithogenic background across the sampling area.

The boxplots for As and Fe indicate the presence of a larger range of data when compared with Ni, Pb, Cr and Cu, with coefficients of variation of 48.3% and 58.8% respectively. The middle values (medians) are near the middle of the boxes, showing that the data is equally spread on either side of the median. Whiskers are longer, indicating that the concentrations of these elements are more variable. This is a moderate variation, indicating that the concentrations of As and Fe are not equal in all the samples. The differences may be attributed to natural variation in the soil or to the presence of increased levels of these elements in some soils (Balasoiu et al., 2001).

The boxplots for Mn and Zn indicate that these elements have the greatest relative variability of all the potentially toxic elements, with coefficients of variation of 70.6% and 54.9% respectively. As the concentration axis is logarithmic, the boxes express proportional rather than absolute spread: Mn ranges from 35.00 to 316.67 ppm, a ninefold difference between the lowest and highest samples, and Zn from 22.33 to 86.00 ppm. Of the two, Zn is the more strongly bottom-weighted: its median of 27.50 ppm lies close to the lower quartile of 24.33 ppm against a maximum of 86.00 ppm, so most values cluster at the low end with a few samples reaching much higher concentrations. For Mn, the median of 112.67 ppm sits nearer the centre of the interquartile range of 52.33 to 151.67 ppm, and the long upper whisker is driven by the highest sample at 316.67 ppm. The high skewness and kurtosis of both elements (1.25 and 1.70 for Mn, 1.86 and 3.26 for Zn) confirm that these distributions are shaped by a small number of markedly enriched samples rather than a general elevation across the study area.

## 4.4. Results of Multivariate Statistical Analysis

### 4.4.1. Spearman's Correlation Matrix

The Spearman's correlation coefficients for the elements of the data set are presented in **Table 9**. Spearman's correlation is a measure of monotonic relationships between two variables. The values are from −1 to 1, with −1 indicating a perfect negative correlation, 1 indicating a perfect positive correlation and 0 indicating no correlation. Coefficients marked * and ** are significant at the 0.05 and 0.01 levels respectively, and coefficients of ±0.79 or above are shown in bold. The strongest correlation recorded among the potentially toxic elements is between Fe and Cu (0.92**), and the correlation between Mn and As is also strong and positive

(0.79**), suggesting that they are related by similar natural or anthropogenic processes such as mining or shared mineral sources. There is also a strong positive correlation between Cu and As (0.73*), which could indicate that they are derived from a shared source or influenced by similar environmental conditions. The strong associations between Cu and Ni (0.74*), Fe and Ni (0.74*) and Mn and Fe (0.70*) suggest that these elements may share a common source of origin. There is a moderate positive correlation between Cr and Pb (0.65*), and a weaker positive correlation between Zn and Pb (0.60), indicating some link between these elements. There is a moderate correlation between Cu and Cr (0.55), indicating that they may share similar sources or environmental activity. There is effectively no correlation between Ni and Zn (0.02), suggesting that they derive from different sources or processes. The correlation between Mn and Cr is very weak and positive (0.15), implying only a minor relationship between the two elements. Al, retained as a lithogenic reference element, correlates negatively with Mn (−0.73*) and Zn (−0.61), indicating that these two elements do not track the aluminosilicate background and are more plausibly controlled by a non-lithogenic input.

**Table 9.** Spearman's correlation matrix.

| Parameters | Al | Si | K | Ti | V | Cr | Mn | Fe | Ni | Cu | Zn | As | Rb | Sr | Y | Zr | Nb | Mo | Pb | Th | U |
|---|---|---|---|---|---|---|---|---|---|---|---|---|---|---|---|---|---|---|---|---|---|
| **Al** | **1.00** | | | | | | | | | | | | | | | | | | | | |
| **Si** | −0.28 | **1.00** | | | | | | | | | | | | | | | | | | | |
| **K** | **0.79**** | −0.50 | **1.00** | | | | | | | | | | | | | | | | | | |
| **Ti** | 0.04 | 0.75* | −0.21 | **1.00** | | | | | | | | | | | | | | | | | |
| **V** | 0.58 | 0.47 | 0.31 | 0.39 | **1.00** | | | | | | | | | | | | | | | | |
| **Cr** | 0.43 | −0.73* | 0.36 | −0.36 | −0.41 | **1.00** | | | | | | | | | | | | | | | |
| **Mn** | −0.73* | −0.37 | −0.42 | −0.56 | **−0.83**** | 0.15 | **1.00** | | | | | | | | | | | | | | |
| **Fe** | −0.21 | −0.73* | −0.02 | **−0.79**** | −0.66* | 0.54 | 0.70* | **1.00** | | | | | | | | | | | | | |
| **Ni** | 0.02 | −0.46 | 0.17 | −0.42 | −0.24 | 0.33 | 0.31 | 0.74* | **1.00** | | | | | | | | | | | | |
| **Cu** | −0.07 | **−0.84**** | 0.24 | −0.77** | −0.66* | 0.55 | 0.60 | **0.92**** | 0.74* | **1.00** | | | | | | | | | | | |
| **Zn** | −0.61 | −0.19 | −0.54 | 0.01 | −0.74* | 0.10 | 0.57 | 0.32 | 0.02 | 0.29 | **1.00** | | | | | | | | | | |
| **As** | −0.49 | −0.53 | 0.02 | −0.73* | −0.65* | 0.01 | **0.79**** | 0.64* | 0.36 | 0.73* | 0.33 | **1.00** | | | | | | | | | |
| **Rb** | **0.81**** | −0.43 | **0.99**** | −0.18 | 0.41 | 0.26 | −0.48 | −0.08 | 0.14 | 0.16 | −0.61 | −0.03 | **1.00** | | | | | | | | |
| **Sr** | 0.72* | 0.32 | 0.40 | 0.50 | **0.87**** | −0.21 | **−0.94**** | −0.74* | −0.39 | −0.62 | −0.51 | −0.71* | 0.46 | **1.00** | | | | | | | |
| **Y** | **−0.79**** | 0.58 | **−0.82**** | 0.36 | −0.36 | −0.33 | 0.45 | −0.19 | −0.36 | −0.36 | 0.41 | 0.01 | **−0.83**** | −0.45 | **1.00** | | | | | | |
| **Zr** | −0.65* | 0.12 | −0.66* | 0.13 | −0.58 | 0.09 | 0.64* | 0.10 | −0.24 | −0.08 | 0.60 | 0.12 | −0.70* | −0.58 | **0.83**** | **1.00** | | | | | |
| **Nb** | 0.09 | 0.47 | −0.13 | 0.77** | 0.18 | 0.05 | −0.32 | −0.48 | −0.30 | −0.58 | −0.04 | −0.70* | −0.10 | 0.18 | 0.39 | 0.41 | **1.00** | | | | |
| **Mo** | −0.57 | 0.11 | −0.57 | 0.26 | −0.58 | 0.14 | 0.46 | 0.34 | 0.37 | 0.20 | 0.62 | 0.03 | −0.61 | −0.61 | 0.55 | 0.62 | 0.43 | **1.00** | | | |
| **Pb** | 0.10 | −0.41 | −0.16 | 0.02 | −0.45 | 0.65* | 0.14 | 0.21 | −0.06 | 0.24 | 0.60 | −0.12 | −0.25 | −0.07 | 0.03 | 0.37 | 0.08 | 0.28 | **1.00** | | |
| **Th** | 0.07 | −0.08 | −0.26 | 0.21 | −0.21 | 0.46 | −0.10 | 0.30 | 0.34 | 0.16 | 0.38 | −0.40 | −0.30 | −0.08 | −0.04 | 0.07 | 0.29 | 0.60 | 0.53 | **1.00** | |
| **U** | −0.47 | 0.44 | −0.23 | 0.60 | −0.26 | −0.39 | 0.07 | −0.36 | −0.24 | −0.26 | 0.36 | 0.01 | −0.23 | −0.19 | 0.53 | 0.35 | 0.50 | 0.50 | −0.16 | −0.03 | **1.00** |

Note: **: Correlation is significant at the 0.01 level (2-tailed). *: Correlation is significant at the 0.05 level (2-tailed).

#### 4.4.2. PCA with Varimax Rotation

Principal Component Analysis (PCA) was performed by extraction on the correlation matrix, with orthogonal Varimax rotation. Five components met the Kaiser criterion (eigenvalue > 1), together accounting for 94.85% of total variance. The complete loading matrix is reported, with loadings ≥ 0.70 shown in bold to mark component-defining variables and those below 0.40 greyed out for clarity; no loadings were suppressed, so squared loadings across each row sum to the reported communality. Negative loadings reflect the opposing pole of a bipolar component, on PC1, for instance, Fe, Ni, and Cu vary inversely with Si, Ti, V, and Sr. Cr, Mn, and Zn carry appreciable cross-loadings and are not cleanly assignable to a single component.

In Table 10, the component resolved the elements into five components. Each component represents a group of elements that vary together, and the accompanying percentage is the share of the total variance it accounts for. PC1 accounts for 30.17% of the total variance and is bipolar: Cu (0.95), Fe (0.93), Ni (0.80) and As (0.65) load positively, while Si (-0.84), Ti (−0.83), Sr (−0.78) and V (−0.70) load negatively. The positive pole groups elements governed by a common source, while the negative pole reflects their dilution by the primary silicate matrix. The grouping indicates that PC1 is strongly influenced by the local geology, in particular the Birimian rocks that underlie the area. The Birimian rocks are known to contain elevated concentrations of Fe, Ni and As, the elements that define this component. Fe and Ni are frequently found in mafic and ultramafic rocks, which are abundant in the Birimian Supergroup. These elements occur naturally, released by the weathering of arsenopyrite and of the iron and nickel-bearing sulphides and silicates of the mafic units. Their concentrations, however, can be raised by human activities (for example, mining) and by environmental factors (for example, soil acidity).

PC2 accounts for 26.75% of the variance and is dominated by Rb (0.99), K (0.95) and Al (0.87). It is interpreted as the aluminosilicate component of the soils, reflecting the distribution of clay and mica phases derived from weathering of the underlying rocks. Its negative pole is carried by Y (−0.78) and Zr (−0.69), so PC2 separates soils dominated by weathered clay and mica from those in which resistant detrital minerals are concentrated. Ni and Cu, which were grouped together in the earlier solution, now load with Fe on PC1.

PC3 explains 14.53% of the total variance and is defined by Th (0.91) against negative loadings for As (−0.72), Mn (−0.67) and Zn (−0.57), separating the resistant thorium-bearing minerals from the more redox-mobile metals. PC4, which explains 11.55% of the variance, is the component most plausibly attributable to anthropogenic activity in the study area. It is defined by Pb (0.96) and Cr (0.74), with a secondary contribution from Zn (0.52), which suggests that these elements are from a shared source or are affected by similar environmental processes. The primary ores of lead and zinc are galena (PbS) and sphalerite (ZnS), respectively, which are exposed in the environment by mining activities. This exposure hastens

their oxidation and releases lead and zinc to the soil. They can also be found with gold-bearing rocks, with further details as to their location in the mining areas. PC5 accounts for the remaining 11.85% of the variance and comprises U (0.82), Nb (0.72), Mo (0.62), Zr (0.54) and Y (0.50), a resistant heavy-mineral association of limited environmental significance in this setting. Communalities range from 0.79 for Ni to 0.99 for several elements, indicating that the five-component solution reproduces almost all of the variance in each element. Cr, Mn and Zn nevertheless load appreciably on more than one component and cannot be attributed to a single source.

**Table 10.** Varimax-rotated component matrix and variance explained for the elements in soils.

| Element | PC1 | PC2 | PC3 | PC4 | PC5 | Communality |
|---|---|---|---|---|---|---|
| Al | −0.24 | **0.87** | 0.33 | 0.12 | −0.19 | 0.98 |
| Si | **−0.84** | −0.39 | 0.11 | −0.27 | 0.21 | 0.99 |
| K | 0.24 | **0.95** | −0.13 | −0.06 | −0.12 | 0.99 |
| Ti | **−0.83** | −0.17 | 0.29 | −0.16 | 0.41 | 0.99 |
| V | **−0.70** | 0.49 | 0.16 | −0.25 | −0.16 | 0.85 |
| Cr | 0.44 | 0.41 | 0.13 | **0.74** | 0.18 | 0.96 |
| Mn | 0.46 | −0.52 | −0.67 | 0.20 | 0.10 | 0.98 |
| Fe | **0.93** | −0.05 | 0.08 | 0.32 | −0.10 | 0.98 |
| Ni | **0.80** | 0.01 | 0.39 | −0.09 | 0.02 | 0.79 |
| Cu | **0.95** | 0.19 | −0.06 | 0.22 | −0.08 | 0.99 |
| Zn | 0.20 | −0.52 | −0.57 | 0.52 | 0.02 | 0.90 |
| As | 0.65 | −0.22 | **−0.72** | −0.02 | −0.06 | 0.99 |
| Rb | 0.09 | **0.99** | −0.04 | 0.04 | −0.05 | 0.99 |
| Sr | **−0.78** | 0.52 | 0.24 | 0.15 | −0.13 | 0.98 |
| Y | −0.18 | **−0.78** | −0.16 | 0.04 | 0.50 | 0.91 |
| Zr | 0.00 | −0.69 | −0.32 | 0.28 | 0.54 | 0.95 |
| Nb | −0.51 | −0.09 | 0.35 | 0.22 | **0.72** | 0.95 |
| Mo | 0.27 | −0.52 | 0.41 | 0.25 | 0.62 | 0.96 |
| Pb | 0.19 | −0.16 | 0.05 | **0.96** | −0.05 | 0.98 |
| Th | 0.14 | −0.08 | **0.91** | 0.20 | 0.08 | 0.90 |
| U | −0.20 | −0.32 | −0.14 | −0.25 | **0.82** | 0.90 |
| *Initial eigenvalue* | 7.41 | 6.72 | 2.97 | 1.70 | 1.13 | |
| *Rotated sum of squared loadings* | 6.34 | 5.62 | 3.05 | 2.43 | 2.49 | |
| *% of total variance* | 30.17 | 26.75 | 14.53 | 11.55 | 11.85 | |
| *Cumulative %* | 30.17 | 56.92 | 71.45 | 83.00 | 94.85 | |

#### 4.4.3. Hierarchical Cluster Analysis

Figure 5 shows the clustering of elements based on their similarities or relation-

ships. It uses Ward's minimum-variance linkage applied to Euclidean distances between the standardised (z-scored) element concentrations, with distances re-scaled to a 0 - 25 range. A cut at approximately 13 on that rescaled scale yields the five-element clusters described below. Distance is labelled on the horizontal axis and refers to the rescaled distance, or how similar or different the elements are. The closer elements are together on the dendrogram, the more similar they are together. The clustering pattern broadly aligns with the factor groupings described above, which lends some mutual support to both analyses, though (as with the PCA) this agreement should be interpreted cautiously, given the small sample size, rather than treated as independent confirmation.

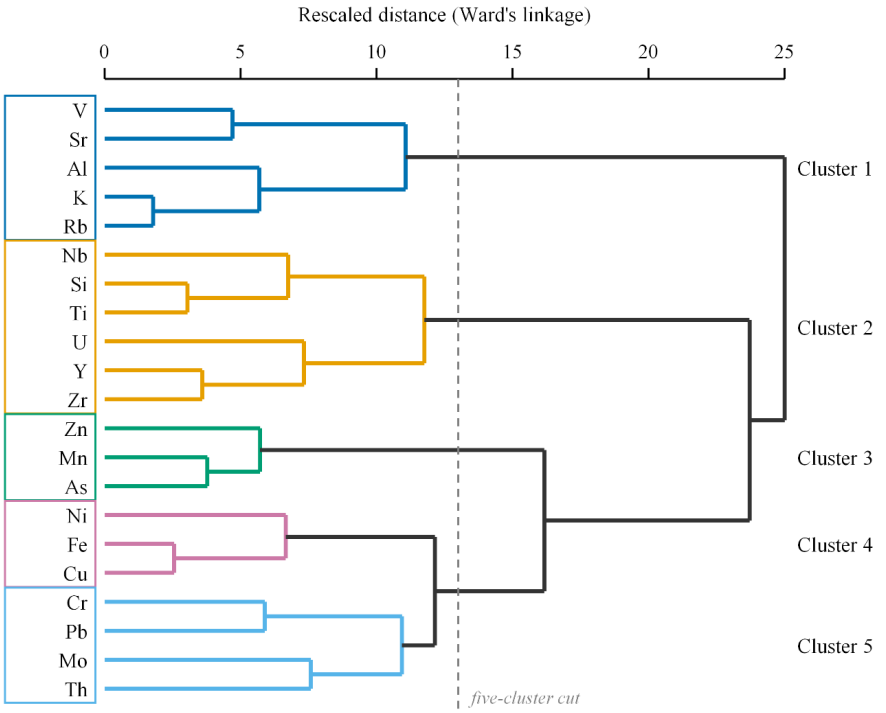


**Figure 5.** Dendrogram from R-mode hierarchical cluster analysis using Ward's linkage on euclidean distances of standardised data (n = 10), showing five element clusters: Cluster 1 (Al-K-Rb-V-Sr), Cluster 2 (Si-Ti-Nb-Y-Zr-U), Cluster 3 (Mn-Zn-As), Cluster 4 (Fe-Ni-Cu) and Cluster 5 (Cr-Pb-Mo-Th). Distances are rescaled to 0 - 25.

Cluster 1 groups Al, K, Rb, V and Sr, and represents the feldspar and mica aluminosilicate matrix of the soils. K and Rb are the closest pair in the entire distance matrix, joining at a rescaled distance of 1.79, with Al attaching at 5.68, while V and Sr pair separately at 4.71 and merge with the Al-K-Rb subgroup at 11.07. The cluster is interpreted as the detrital silicate framework of the soils and corresponds to the positive pole of PC2.

Cluster 2 comprises Si, Ti, Nb, Y, Zr and U, a resistant heavy-mineral suite of quartz, rutile, zircon and monazite-type phases. Si and Ti join at 3.05 and Y and Zr at 3.58, with Nb attaching to Si-Ti at 6.75 and U to Y-Zr at 7.33, the two subgroups merging at 11.76; these are physically and chemically resistant minerals of

geogenic origin. Cluster 3 is formed by Mn, Zn and As, with Mn and As joining at 3.78 and Zn added at 5.72, and is interpreted as an association of As and Zn scavenged by manganese oxides. The Birimian rocks are thought to contain considerable amounts of Mn and As, which are grouped together in this cluster. These are naturally occurring and result from the weathering of arsenopyrite and manganese oxides in the Birimian rocks, but concentrations are probably higher because of the mining operations, which bring the minerals into contact with the environment and the acidic environment that results.

Cluster 4 groups Fe, Ni and Cu, an association hosted by iron oxides and sulphide phases. Fe and Cu form the second closest pair in the distance matrix, joining at 2.55, with Ni added at 6.66. This cluster corresponds exactly to the positive pole of PC1 and to the Fe-Cu correlation of 0.92** in Table 9. Cluster 5 contains Cr, Pb, Mo and Th. Cr and Pb join at 5.89 and Mo and Th at 7.58, the two pairs merging at 10.93. The Cr-Pb pairing is interpreted as a discrete input, probably anthropogenic, distinct from both the silicate matrix and the iron-oxide association, and it reproduces the Pb-Cr grouping recovered as PC4 in the factor analysis.

At higher levels of the dendrogram, Clusters 4 and 5 merge at 12.14 and then join Cluster 3 at 16.16 to form a broad metal-bearing supergroup, whereas Clusters 1 and 2 remain separate from that supergroup until rescaled distances of 23.71 and 25.00. The primary division in the data is therefore between the lithogenic silicate and heavy-mineral assemblage and the metal-bearing assemblage. Because the analysis rests on ten samples, cluster membership at the margins, particularly for Mo, Th, U and Nb, would be sensitive to the addition of further samples. The dendrogram is accordingly best read as indicative of element associations rather than as a definitive classification.

## 4.5. Analysis of PTEs Pollution Assessment

### 4.5.1. Results of Geo-Accumulation Index (Igeo)

The results of the geoaccumulation index are presented in Table 11. Seventeen of the twenty-one elements return negative mean Igeo values and fall under Class 0, among them Zn (−2.09), Mn (−3.70), Ni (−2.24), Cu (−1.40), Pb (−1.14), Fe (−1.17) and Cr (−0.75), indicating that their concentrations are below pollution thresholds. This means that the soil is not polluted with respect to these metals, and their levels are within natural background ranges. Zr (0.33), Nb (0.28) and Mo (0.55) return slightly positive mean values and fall under Class 1, unpolluted to moderately polluted. All three are associated with the resistant heavy-mineral phases identified in the cluster analysis rather than with any anthropogenic source, so this marginal enrichment is most likely lithogenic. As has the highest Igeo value among the metals. It falls under Class 2, moderately polluted. Arsenic is the only element to reach a polluting classification, and it does so at every sample location, with individual values ranging from 0.68 to 2.98 and the maximum, at location D1, falling in Class 3, moderately to heavily polluted. This suggests that arsenic levels are significantly higher than natural background levels, likely due to con-

tamination from activities such as mining. Mean Igeo values greater than zero are shown in bold in Table 11, and classes are assigned from the mean across the ten sample locations. Thorium at one location and uranium at six locations returned concentrations below the detection limit of the instrument; Igeo is undefined for a zero concentration, so those samples are excluded from the statistics for these two elements and they should be read as below detection rather than as unpolluted.

Table 11. Geo-accumulation Index (Igeo) of elements determined in soils of the study.

| Element | Minimum | Maximum | Mean | SD | Igeo Class (Mean) | Locations with Igeo > 0 |
|---|---|---|---|---|---|---|
| Al | −1.00 | −0.15 | −0.51 | 0.32 | 0—Unpolluted | 0 of 10 |
| Si | −0.70 | −0.44 | −0.54 | 0.10 | 0—Unpolluted | 0 of 10 |
| K | −2.92 | −1.62 | −2.32 | 0.46 | 0—Unpolluted | 0 of 10 |
| Ti | −0.38 | 0.18 | −0.06 | 0.24 | 0—Unpolluted | 5 of 10 |
| V | −2.13 | −1.46 | −1.79 | 0.18 | 0—Unpolluted | 0 of 10 |
| Cr | −1.58 | −0.16 | −0.75 | 0.40 | 0—Unpolluted | 0 of 10 |
| Mn | −5.19 | −2.01 | −3.70 | 1.04 | 0—Unpolluted | 0 of 10 |
| Fe | −2.47 | 0.00 | −1.17 | 0.93 | 0—Unpolluted | 0 of 10 |
| Ni | −2.67 | −1.81 | −2.24 | 0.24 | 0—Unpolluted | 0 of 10 |
| Cu | −1.85 | −0.89 | −1.40 | 0.37 | 0—Unpolluted | 0 of 10 |
| Zn | −2.67 | −0.73 | −2.09 | 0.65 | 0—Unpolluted | 0 of 10 |
| As | 0.68 | 2.98 | **1.89** | 0.75 | 2—Moderately polluted | 10 of 10 |
| Rb | −2.32 | −1.34 | −1.87 | 0.37 | 0—Unpolluted | 0 of 10 |
| Sr | −3.20 | −1.71 | −2.51 | 0.52 | 0—Unpolluted | 0 of 10 |
| Y | −0.78 | 0.13 | −0.37 | 0.30 | 0—Unpolluted | 1 of 10 |
| Zr | −0.13 | 0.80 | **0.33** | 0.31 | 1—Unpolluted to moderate | 8 of 10 |
| Nb | −0.07 | 0.52 | **0.28** | 0.19 | 1—Unpolluted to moderate | 9 of 10 |
| Mo | −0.96 | 1.26 | **0.55** | 0.65 | 1—Unpolluted to moderate | 9 of 10 |
| Pb | −1.63 | −0.66 | −1.14 | 0.31 | 0—Unpolluted | 0 of 10 |
| Th | −1.75 | −0.40 | −0.89 | 0.48 | 0—Unpolluted | 0 of 10 |
| U | −2.06 | −1.06 | −1.81 | 0.50 | 0—Unpolluted | 0 of 10 |

#### 4.5.2. Results of Enrichment Factor (EF)

The enrichment factor for the PTEs is presented in Table 12. Nineteen of the twenty-one elements return mean EF values below 2, indicating deficiency to minimal enrichment. Their concentrations are close to natural background levels relative to aluminium and they do not pose a significant pollution risk. Molybdenum is the exception among the remaining elements, with a mean EF of 2.38, placing it in the moderate category, and it exceeds EF 2 at six of the ten locations. Arsenic has a mean EF of 6.39, placing it in the significant enrichment category, and it exceeds EF 2 at nine of the ten locations, rising to 15.80 at location D1. No element reaches

EF 20 anywhere in the study area, so none is very highly or extremely enriched. This is likely from exposure of arsenopyrite to the atmosphere because of mining.

Table 12. Aluminium-normalised enrichment factors of elements determined in soils of the study area.

| Element | Minimum | Maximum | Mean | SD | Enrichment Category (Mean) | Locations with EF > 2 |
|---|---|---|---|---|---|---|
| Al | 1.00 | 1.00 | 1.00 | 0.00 | Reference element | Reference element |
| Si | 0.72 | 1.39 | 1.00 | 0.26 | Deficiency to minimal | 0 of 10 |
| K | 0.20 | 0.40 | 0.29 | 0.06 | Deficiency to minimal | 0 of 10 |
| Ti | 0.89 | 2.15 | 1.41 | 0.39 | Deficiency to minimal | 1 of 10 |
| V | 0.32 | 0.53 | 0.42 | 0.07 | Deficiency to minimal | 0 of 10 |
| Cr | 0.50 | 1.37 | 0.88 | 0.27 | Deficiency to minimal | 0 of 10 |
| Mn | 0.03 | 0.50 | 0.16 | 0.15 | Deficiency to minimal | 0 of 10 |
| Fe | 0.20 | 1.81 | 0.79 | 0.50 | Deficiency to minimal | 0 of 10 |
| Ni | 0.18 | 0.42 | 0.31 | 0.08 | Deficiency to minimal | 0 of 10 |
| Cu | 0.31 | 0.87 | 0.57 | 0.19 | Deficiency to minimal | 0 of 10 |
| Zn | 0.17 | 1.21 | 0.41 | 0.32 | Deficiency to minimal | 0 of 10 |
| As | 1.78 | 15.80 | **6.39** | 4.22 | Significant | 9 of 10 |
| Rb | 0.30 | 0.46 | 0.39 | 0.05 | Deficiency to minimal | 0 of 10 |
| Sr | 0.19 | 0.34 | 0.26 | 0.06 | Deficiency to minimal | 0 of 10 |
| Y | 0.67 | 2.11 | 1.19 | 0.52 | Deficiency to minimal | 1 of 10 |
| Zr | 1.05 | 3.48 | 1.94 | 0.87 | Deficiency to minimal | 3 of 10 |
| Nb | 1.21 | 2.76 | 1.77 | 0.48 | Deficiency to minimal | 2 of 10 |
| Mo | 0.68 | 4.61 | **2.38** | 1.20 | Moderate | 6 of 10 |
| Pb | 0.42 | 1.16 | 0.67 | 0.24 | Deficiency to minimal | 0 of 10 |
| Th | 0.00 | 1.35 | 0.72 | 0.40 | Deficiency to minimal | 0 of 10 |
| U | 0.00 | 0.93 | 0.20 | 0.31 | Deficiency to minimal | 0 of 10 |

#### 4.5.3. Results of Contamination Factor (CF)

In Table 13, Zn, Mn, Cu, Pb, Ni and Cr all have mean CF values below 1 (0.39, 0.14, 0.59, 0.69, 0.32 and 0.92 respectively), indicating low contamination. Their concentrations are within natural background levels, and they do not pose any significant pollution risk. Neither Pb nor Ni exceeds CF 1 at any location, and Cr does so at four of the ten locations without its mean reaching the moderate class. As has a CF value greater than 6, indicating very high contamination. This suggests significant pollution, likely from exposure of arsenopyrite to the atmosphere because of mining. Arsenic is the only element in the very high class, with a mean of 6.22 and a maximum of 11.82 at location D1, and it exceeds CF 1 at all ten locations. Ti, Zr and Nb also exceed CF 1 at every location but remain within the moderate class and are interpreted as lithogenic, being resistant heavy-mineral constituents that group together in the cluster analysis; Mo is moderate at nine of

the ten locations. Al, Si and Y return mean CF values only slightly above unity (1.08, 1.03 and 1.18). These are matrix constituents rather than pollutants, and values close to 1 indicate that the soils are compositionally similar to average shale, which supports the use of average shale as the reference composition for this study area.

Table 13. Summary of contamination factor for the elements.

| Element | Minimum | Maximum | Mean | SD | Contamination Class (Mean) | Locations with CF > 1 |
|---|---|---|---|---|---|---|
| Al | 0.75 | 1.35 | **1.08** | 0.23 | Moderate | 7 of 10 |
| Si | 0.92 | 1.11 | **1.03** | 0.07 | Moderate | 6 of 10 |
| K | 0.20 | 0.49 | 0.31 | 0.10 | Low | 0 of 10 |
| Ti | 1.15 | 1.69 | **1.46** | 0.24 | Moderate | 10 of 10 |
| V | 0.34 | 0.55 | 0.44 | 0.06 | Low | 0 of 10 |
| Cr | 0.50 | 1.34 | 0.92 | 0.24 | Low | 4 of 10 |
| Mn | 0.04 | 0.37 | 0.14 | 0.10 | Low | 0 of 10 |
| Fe | 0.27 | 1.50 | 0.79 | 0.47 | Low | 3 of 10 |
| Ni | 0.24 | 0.43 | 0.32 | 0.05 | Low | 0 of 10 |
| Cu | 0.41 | 0.81 | 0.59 | 0.15 | Low | 0 of 10 |
| Zn | 0.24 | 0.91 | 0.39 | 0.21 | Low | 0 of 10 |
| As | 2.41 | 11.82 | **6.22** | 3.01 | Very high | 10 of 10 |
| Rb | 0.30 | 0.59 | 0.42 | 0.11 | Low | 0 of 10 |
| Sr | 0.16 | 0.46 | 0.28 | 0.10 | Low | 0 of 10 |
| Y | 0.87 | 1.64 | **1.18** | 0.25 | Moderate | 7 of 10 |
| Zr | 1.37 | 2.60 | **1.92** | 0.42 | Moderate | 10 of 10 |
| Nb | 1.42 | 2.15 | **1.83** | 0.23 | Moderate | 10 of 10 |
| Mo | 0.77 | 3.59 | **2.37** | 0.86 | Moderate | 9 of 10 |
| Pb | 0.48 | 0.95 | 0.69 | 0.15 | Low | 0 of 10 |
| Th | 0.00 | 1.14 | 0.76 | 0.35 | Low | 3 of 10 |
| U | 0.00 | 0.72 | 0.18 | 0.25 | Low | 0 of 10 |

## 4.6. Pollution Load Index and Potential Ecological Risk Index

### 4.6.1. Pollution Load Index

The pollution load index of the study area (Table 14) gives a study-area pollution load index of 0.599, calculated as the geometric mean of the ten site values. Every location returns a PLI below unity, ranging from 0.397 at A2 to 0.897 at E1, so no site exceeds the baseline value of 1.0 and the soils are classed as unpolluted on this index throughout the study area. While most elements contribute minimally to the pollution, As is the primary contributor and requires further investigation and management to reduce its environmental impact.

### 4.6.2. Potential Ecological Risk Index

The single-element risk factors and site-level indices are presented in Tables 14(a)-

(b). The ecological risk index averages 72.61 across the ten locations and ranges from 33.38 at A2 to 129.28 at D1 (Table 14(b)). All ten values fall below the conventional threshold of 150 for low risk; on a scale adjusted for the sum of the toxic-response factors, which accounts for the seven elements assessed here rather than the eight of the original formulation. Hakanson's conventional boundaries of 150, 300 and 600 were calibrated for eight pollutants with a toxic-response factor sum of 133; the seven elements assessed here sum to 29, so those thresholds cannot be reached by construction and would return low risk at every location. Rescaling them in proportion gives boundaries of 32.7, 65.4 and 130.8, on which the four locations in the A and B transects are of moderate risk and the remaining six, including D1 at 129.28, are of considerable risk. Arsenic accounts for 85.7% of the total risk on average. Arsenic is by far the dominant contributor, with a risk factor of 62.23, and is accordingly the element of principal concern in the study area. It should be noted that cadmium and mercury were not among the elements determined by XRF in this study. Both carry the highest toxic-response factors in Hakanson's formulation, 30 and 40 respectively against 10 for arsenic, so the risk index reported here rests on seven elements only and represents a lower bound on the true ecological risk rather than a complete assessment. The next largest contributions come from Pb (3.47), Cu (2.93), Cr (1.85) and Ni (1.61), all of which are an order of magnitude below arsenic. Zn (0.39) and Mn (0.14) contribute negligibly to the overall risk.

Table 14. Summary of PLI and RI for the elements.

**(a) Single-element Risk Factors**

| Element | Tr | Mean CF | Mean Er | Minimum Er | Maximum Er | Risk Class (Mean Er) |
|---|---|---|---|---|---|---|
| Zn | 1 | 0.39 | 0.39 | 0.24 | 0.91 | Low risk |
| Pb | 5 | 0.69 | 3.47 | 2.42 | 4.75 | Low risk |
| As | 10 | 6.22 | **62.23** | 24.10 | 118.21 | Moderate risk |
| Ni | 5 | 0.32 | 1.61 | 1.18 | 2.13 | Low risk |
| Mn | 1 | 0.14 | 0.14 | 0.04 | 0.37 | Low risk |
| Cr | 2 | 0.92 | 1.85 | 1.00 | 2.69 | Low risk |
| Cu | 5 | 0.59 | 2.93 | 2.07 | 4.04 | Low risk |
| *Sum* | *29* | | *72.61* | | | |

**(b) Site-level Indices by Sample Location**

| Sample Location | PLI | PLI Classification | RI | RI Classification | As Share of RI (%) |
|---|---|---|---|---|---|
| A1 | 0.420 | Unpolluted (baseline) | 39.82 | Moderate risk | 76.0 |
| A2 | 0.397 | Unpolluted (baseline) | 33.38 | Moderate risk | 72.2 |
| B1 | 0.439 | Unpolluted (baseline) | 44.84 | Moderate risk | 82.3 |
| B2 | 0.454 | Unpolluted (baseline) | 49.54 | Moderate risk | 82.3 |
| C1 | 0.637 | Unpolluted (baseline) | 97.85 | Considerable risk | 90.4 |
| C2 | 0.702 | Unpolluted (baseline) | 93.09 | Considerable risk | 87.3 |
| D1 | 0.856 | Unpolluted (baseline) | 129.28 | Considerable risk | 91.4 |

Continued

| | | | | | |
|---|---|---|---|---|---|
| D2 | 0.614 | Unpolluted (baseline) | 72.08 | Considerable risk | 87.2 |
| E1 | 0.897 | Unpolluted (baseline) | 94.07 | Considerable risk | 86.1 |
| E2 | 0.844 | Unpolluted (baseline) | 72.21 | Considerable risk | 81.0 |
| *Study area* | 0.599 | Unpolluted (baseline) | 72.61 | Considerable risk | 85.7 |

### 4.7.Arsenic Contamination: Multi-Index Assessment and Source Apportionment

Arsenic contamination in the study area using multi-pollution index assessment is presented in Tables 15(a)-(b). The soils of Adaase are polluted with respect to a single element. Arsenic averages 80.90 ppm against an average-shale background of 13 ppm (range 31.33 - 153.67 ppm, SD 39.07), giving a mean contamination factor of 6.22 ("very high"), a mean geoaccumulation index of 1.89 (Class 2, moderately polluted) and a mean Al-normalised enrichment factor of 6.39 ("significant"). Contamination factor and Igeo place As above threshold at all ten locations, EF at nine and the ecological risk factor at seven; arsenic contributes 72.2% - 91.4% (mean 85.7%) of the ecological risk index at every site, and no other element exceeds the low-risk band anywhere. The apparent conflict between indices is a property of their formulations, Igeo compresses the scale through a 1.5 background correction and a $\log_2$ transform, and PLI dilutes one enriched element across the geometric mean of eight, rather than a contradiction; the low pooled PLI of 0.599 should therefore not be read as evidence of an unpolluted area.

Table 15. Arsenic in soils of the study area: pollution indices and statistical corroboration.

**(a) Arsenic across the Pollution Indices**

| Index | Minimum | Maximum | Mean | SD | Classification (Mean) | Locations Exceeding Threshold |
|---|---|---|---|---|---|---|
| Concentration (ppm) | 31.33 | 153.67 | 80.90 | 39.07 | CV 48.3% | - |
| Contamination factor (CF) | 2.41 | 11.82 | 6.22 | 3.01 | Very high | 10 of 10 exceed |
| Geo-accumulation Index (Igeo) | 0.68 | 2.98 | 1.89 | 0.75 | 2—Moderately polluted | 10 of 10 exceed |
| Enrichment factor (EF, Al-normalised) | 1.78 | 15.80 | 6.39 | 4.22 | Significant | 9 of 10 exceed |
| Ecological risk factor (Er) | 24.10 | 118.21 | 62.23 | | Moderate risk | 7 of 10 exceed |

**(b) Statistical Corroboration of the Arsenic Anomaly**

| Statistical Evidence | Result | Interpretation |
|---|---|---|
| Descriptive statistics (Table 7) | Mean 80.90 ppm, range 31.33 - 153.67, SD 39.07, CV 48.3%, skewness +0.47 | A coefficient of variation near 50% with positive skew indicates a heterogeneous, point-source-influenced distribution rather than a uniform lithogenic background. |

**Continued**

| | | |
|---|---|---|
| Spearman correlation (Table 8) | As-Mn +0.79, As-Cu +0.73, As-Fe +0.64; As-Ti −0.73, As-Sr −0.71, As-Nb −0.70, As-V −0.65 | Arsenic co-varies positively with the Mn- and Fe-oxide and sulphide-associated metals and inversely with the resistate silicate matrix, consistent with a secondary, non-detrital host phase. |
| Principal component analysis (Table 9) | Loads −0.72 on PC3 with Mn (−0.67) and Zn (−0.57); communality 0.99 | Arsenic defines the negative pole of PC3, a component that opposes the Th-bearing resistate minerals. Its behaviour is not explained by the two lithogenic components PC1 and PC2. |
| Hierarchical cluster analysis (Figure 5) | Joins Mn at a rescaled distance of 3.78, with Zn added at 5.72 to form Cluster 3 | Cluster 3 (Mn-Zn-As) is recovered identically by the factor and cluster analyses, so the association is stable to the choice of multivariate method. |
| Spatial pattern (Table 13) | Every index peaks at D1: CF 11.82, Igeo 2.98, EF 15.80, Er 118.21; minima at A1 and A2 | The four indices agree on the spatial ranking despite different formulations and normalisers, indicating a real gradient rather than an artefact of any one index. |
| Contribution to ecological risk (Table 13) | 72.2% to 91.4% of RI at every location, mean 85.7% | Arsenic dominates the ecological risk at all ten locations, and no other element exceeds the low-risk band anywhere. |

Geochemistry separates lithogenic from anthropogenic control. Arsenic correlates positively with Mn (+0.79), Cu (+0.73) and Fe (+0.64) and negatively with the resistant silicate suite Ti (−0.73), Sr (−0.71), Nb (−0.70) and V (−0.65), and it defines the negative pole of PC3 (loading −0.720; communality 0.990) alongside Mn and Zn, a component independent of the two lithogenic components PC1 and PC2. Hierarchical clustering recovers the same Mn-Zn-As group (As joining Mn at a Ward distance of 1.477), so the association is stable to the choice of method. A coefficient of variation near 50% with positive skew (+0.47) and a single pronounced maximum at D1 (CF 11.82, Igeo 2.98, EF 15.80, Er 118.21) against minima at A1/A2 indicates a point-source-influenced, heterogeneous distribution rather than uniform geogenic enrichment. This is consistent with the geological setting: the Birimian metavolcanic and metasedimentary rocks of the Ashanti belt host gold in arsenopyrite-bearing sulphide ore, so weathering of mineralised bedrock supplies a naturally elevated baseline, while ore processing, tailings and artisanal workings redistribute As onto surface soils where it is scavenged by secondary Mn-Fe oxide phases, the non-detrital host implied by the correlation and factor structure.

The pH-arsenic relationship observed here reflects a between-area rather than a within-site control. Areas A and B are acidic (pH 4.80 - 5.04) and uniformly low in As (31 - 53 ppm), whereas Areas C, D and E are less acidic (pH 5.18 - 6.96) and uniformly higher in As (76 - 154 ppm). This pattern is consistent with the behav-

iour of arsenic as a predominantly anionic species in soil: unlike cationic trace elements, whose sorption to sesquioxide surfaces weakens as pH falls. Arsenate mobility and availability increase as pH rises, because the positive surface charge of Fe/Mn/Al oxides, and hence their capacity to retain anionic As diminishes at higher pH (Mensah et al., 2025). This anion-specific response distinguishes arsenic from the cationic metals discussed above (Mn, Zn, Cu, Ni, Pb), which remained below guideline values across all areas and would be expected to show the opposite pH sensitivity. Elevated pH in the less acidic zones is also consistent with proximity to reclaimed or historically disturbed tailings material. Boateng et al. (2012) reported that ex-tailings soils at the AngloGold Obuasi concession carried substantially higher pH (7.6 - 8.4) than undisturbed control soil (pH 6.0), reflecting the neutralising effect of tailings substrate and reclamation amendments. That mining disturbance in the wider Obuasi area is associated with elevated, spatially structured arsenic contamination is further corroborated at the groundwater interface by Ankapong et al. (2025), who linked arsenic exceedances in groundwater at Sanso, within the Obuasi municipal district, to mining-related sources. These studies support the interpretation that pH and arsenic respond jointly to a common spatial factor, proximity to mining disturbance, with pH acting mechanistically on the stability of the oxide phases that host arsenic, rather than reflecting a direct within-site causal control.

The contribution of this study is methodological as much as descriptive. Rather than reporting a single index, it applies five (concentration, CF, Igeo, Al-normalised EF, Er/RI) to the same locations on a common background and demonstrates that they agree on the spatial ranking while diverging in absolute class, and it explains that divergence analytically, providing a template for reconciling indices that are routinely reported as though interchangeable. It further couples the index results to correlation, PCA and hierarchical clustering so that the arsenic anomaly is corroborated by three independent lines of statistical evidence, and it quantifies arsenic's dominance of ecological risk at the location scale rather than as a study-area average. The limits are stated: Cd and Hg were not determined by XRF and carry the highest toxic-response factors (30 and 40 against 10 for As), so RI is a lower bound; with n = 10, the multivariate results are exploratory, and the agreement of PCA and HCA reflects internal consistency of one correlation structure rather than independent replication.

## 5. Conclusion

This study assessed the levels of Potentially Toxic Elements (PTEs) in soils around artisanal mining sites in the Adaase community in Obuasi. The results showed that arsenic (As) is the primary PTE in the area, with a mean concentration of 80.90 ppm across the ten locations, some six times the average background of 13 ppm, posing significant environmental and health risks. The other elements (Mn, Cr, Ni, Cu, Pb and Zn) returned mean contamination factors below 1 and negative mean geoaccumulation indices, and are better understood as reflecting the natural

composition of the soils. The mean CF of arsenic, 6.22, falls in the very high contamination class and exceeds 1 at all ten locations, whereas Pb, Zn, Mn, Cr, Cu and Ni remain below 1 throughout and are classed as low contamination. The mean Igeo of arsenic, 1.89, places it in Müller Class 2, moderately polluted, rising to 2.98 at location D1 in Class 3, while the other elements (Pb, Zn, Mn, Cr, Cu, Ni) all return negative values in Class 0. The mean aluminium-normalised EF of arsenic, 6.39, places it in the significant enrichment category, while the other elements (Pb, Zn, Mn, Cr, Cu, Ni) fell in the deficiency to minimal enrichment category. The pollution load index remained below unity at every location, with a study-area value of 0.599, so the soils show no overall deterioration in quality on that measure; the potential ecological risk index, however, averaged 72.61 and ranged from 33.38 to 129.28, with six of the ten locations in the considerable risk band and arsenic accounting for between 72.2% and 91.4% of the risk at each. The two indices diverge because the pollution load index averages arsenic against seven elements at or below background, whereas the risk index weights it by a toxic-response factor of 10; the low pollution load index should not therefore be read as evidence of uncontaminated soils. Cadmium and mercury were not determined in this study and carry higher toxic-response factors than arsenic, so the reported risk index is a lower bound.

Arsenic contamination is largely influenced by the geology of the area, particularly the weathering of arsenopyrite in the Birimian rocks, but mining activities have further increased its levels by exposing arsenopyrite to the environment. Manganese and zinc group with arsenic in both the factor and cluster analyses, indicating a shared association with manganese-oxide phases, while iron, nickel and copper form a separate group consistent with mafic and sulphide sources in the Birimian rocks. Chromium and lead form a discrete pairing that is not explained by either lithogenic component and is the grouping most plausibly attributable to mining activity. These elements are distributed in the soils due to the combined effect of natural geology and mining.

The major Potentially Toxic Element (PTE) of concern in the study area is arsenic (As). This will require frequent monitoring of soil and water for arsenic concentrations. It will assist in monitoring contamination patterns and uncover hotspot areas for contamination. Chemical stabilisation should be used to aid in the immobilization of arsenic, thus making the soil less mobile and more suitable for agriculture and less contaminating to human health.

## Author Contributions

Conceptualization, A.A.A. and J.S.; methodology, A.A.A., B.S.D., C.A.G. and A.K.K.; software, J.S., A.K.K. and B.S.D.; validation, A.A.A., A.K.K., and B.S.D.; formal analysis, A.A.A., A.K.K. and B.S.D.; investigation, B.S.D. and C.A.G.; resources, A.A.A., B.S.D. and C.A.G.; data curation, B.S.D. and C.A.G.; writing—original draft preparation, A.K.K. and B.S.D.; writing—review and editing, A.A.A., A.K.K. and B.S.D.; visualization, A.A.A. and A.K.K.; supervision, A.A.A.; project administration, A.A.A.; funding acquisition, A.A.A., B.S.D. and C.B.G. All authors have read and

agreed to the published version of the manuscript.

## Conflicts of Interest

The authors declare no conflicts of interest regarding the publication of this paper.

## References

Abdul-Wahab, S. A., & Marikar, F. (2012). The Environmental Impact of Gold Mines: Pollution by Heavy Metals. *Open Engineering, 2,* 304-313. https://doi.org/10.2478/s13531-011-0052-3

Ackerman, J. J. H., Grove, T. H., Wong, G. G., Gadian, D. G., & Radda, G. K. (1980). Mapping of Metabolites in Whole Animals by 31P NMR Using Surface Coils. *Nature, 283,* 167-170. https://doi.org/10.1038/283167a0

Adomako, T., & Ampadu, B. (2015). The Impact of Agricultural Practices on Environmental Sustainability in Ghana: A Review. *Journal of Sustainable Development, 8,* 70-85. https://doi.org/10.5539/jsd.v8n8p70

Adu-Poku, I., Drummond, J., & Li, Z. (2012). Land-Cover Change Monitoring in Obuasi, Ghana: An Integration of Earth Observation, Geoinformation Systems and Stochastic Modelling. *Journal of Earth Science and Engineering, 2,* 1-14.

Akoto, O., Bortey-Sam, N., Nakayama, S. M. M., Ikenaka, Y., Baidoo, E., Apau, J. et al. (2018). Characterization, Spatial Variation and Risk Assessment of Heavy Metals and a Metalloid in Surface Soils in Obuasi, Ghana. *Journal of Health and Pollution, 8,* Article 1809. https://doi.org/10.5696/2156-9614-8.19.180902

Anarfi, K., Hill, R. A., & Shiel, C. (2020). Highlighting the Sustainability Implications of Urbanisation: A Comparative Analysis of Two Urban Areas in Ghana. *Land, 9,* Article 300. https://doi.org/10.3390/land9090300

Ankapong, M., Ashong, G. W., Adjaottor, A. A., Ababio, B. A., Kwaansa-Ansah, E. E., & Toku, M. (2025). Assessment and Management of Arsenic Contamination in Groundwater from Sanso, Ghana: Health Risk Implications, Source Identification, Adsorption and Immobilization for Safe Disposal. *Toxicology Reports, 15,* Article 102157. https://doi.org/10.1016/j.toxrep.2025.102157

Balasoiu, C., Zagury, G., & Deschenes, L. (2001). Partitioning and Speciation of Chromium, Copper, and Arsenic in CCA-Contaminated Soils: Influence of Soil Composition. *The Science of The Total Environment, 280,* 239-255. https://doi.org/10.1016/s0048-9697(01)00833-6

Bartrem, C., Tirima, S., von Lindern, I., von Braun, M., Worrell, M. C., Mohammad Anka, S. et al. (2014). Unknown Risk: Co-Exposure to Lead and Other Heavy Metals among Children Living in Small-Scale Mining Communities in Zamfara State, Nigeria. *International Journal of Environmental Health Research, 24,* 304-319. https://doi.org/10.1080/09603123.2013.835028

Baveye, P. C., Otten, W., Kravchenko, A., Balseiro-Romero, M., Beckers, É., Chalhoub, M. et al. (2018). Emergent Properties of Microbial Activity in Heterogeneous Soil Microenvironments: Different Research Approaches Are Slowly Converging, Yet Major Challenges Remain. *Frontiers in Microbiology, 9,* Article ID: 1929. https://doi.org/10.3389/fmicb.2018.01929

Bempah, C. K., & Ewusi, A. (2016). Heavy Metals Contamination and Human Health Risk Assessment around Obuasi Gold Mine in Ghana. *Environmental Monitoring and Assessment, 188,* 1-13. https://doi.org/10.1007/s10661-016-5241-3

Benarabi, A., Nili, M. S., & Douadi, A. (2021). Study of Some Indicators of Environmental

Pollution of Surface Soil for the City of Touggourt (*Southeast algeria*). *Nature Environment and Pollution Technology, 20,* 1863-1871. https://doi.org/10.46488/nept.2021.v20i05.001

Boateng, E., Dowuona, G. N. N., Nude, P. M., Foli, G., Gyekye, P., & Hashim, M. (2012). Geochemical Assessment of the Impact of Mine Tailings Reclamation on the Quality of Soils at AngloGold Concession, Obuasi, Ghana. *Research Journal of Environmental and Earth Sciences, 4,* 466-474.

Borges, E. M. (2023). Data Visualization Using Boxplots: Comparison of Metalloid, Metal, and Nonmetal Chemical and Physical Properties. *Journal of Chemical Education, 100,* 2809-2817. https://doi.org/10.1021/acs.jchemed.3c00207

CCME (2007). *Canadian Soil Quality Guidelines for the Protection of Environmental and Human Health: Summary Tables. Canadian Council of Ministers of the Environment* (7 p).

Danala Danga, S., Ekengele Nga, L., Tiki, D., Mamdem, L. E., Djangue Moustapha, B., Ibrahim, B. A. et al. (2025). Speciation and Bioavailability of Potentially Toxic Element in Soils and Sediments of Mining Areas in Meiganga Adamawa Plateau (Cameroon). *Environmental Geochemistry and Health, 47,* Article No. 398. https://doi.org/10.1007/s10653-025-02716-1

Darko Asamoah, B., Yevugah, L. L., Borquaye, L. S., Dodd, M., & Darko, G. (2024). Spatial Distribution, Bioaccessibility, and Human Health Implications of Potentially Toxic Elements in Mining-Impacted Topsoils in Obuasi Municipality of Ghana. *Environmental Geochemistry and Health, 46,* Article No. 291. https://doi.org/10.1007/s10653-024-02028-w

Darko, G., Boakye, K. O., Nkansah, M. A., Gyamfi, O., Ansah, E., Yevugah, L. L. et al. (2019). Human Health Risk and Bioaccessibility of Toxic Metals in Topsoils from Gbani Mining Community in Ghana. *Journal of Health and Pollution, 9,* Article 190602. https://doi.org/10.5696/2156-9614-9.22.190602

de Souza, E. S., Texeira, R. A., da Costa, H. S. C., Oliveira, F. J., Melo, L. C. A., do Carmo Freitas Faial, K. et al. (2017). Assessment of Risk to Human Health from Simultaneous Exposure to Multiple Contaminants in an Artisanal Gold Mine in Serra Pelada, Pará, Brazil. *Science of The Total Environment, 576,* 683-695. https://doi.org/10.1016/j.scitotenv.2016.10.133

Donkor, A. K., Nartey, V. K., Bonzongo, J. C., & Adotey, D. K. (2006). Artisanal Mining of Gold with Mercury in Ghana. *West African Journal of Applied Ecology, 9,* 1-8. https://doi.org/10.4314/wajae.v9i1.45666

Ewusi, A., Tetteh, S. E. K., Klu, A. K., & Seidu, J. (2023). Hydrogeochemical Analysis of Water in the Ayanfuri Area: Implications for Human Consumption and Irrigation. *Earth Science Malaysia, 7,* 142-155. https://doi.org/10.26480/esmy.02.2023.142.155

Fosu-Mensah, B. Y., Ofori, A., Ofosuhene, M., Ofori-Attah, E., Nunoo, F. E., Darko, G., Tuffour, I., Gordon, C., Arhinful, D. K., Nyarko, A. K., & Appiah-Opong, R. (2018). Assessment of Heavy Metal Contamination and Distribution in Surface Soils and Plants along the West Coast of Ghana. *West African Journal of Applied Ecology, 26,* 167-178.

Gololobova, A., & Legostaeva, Y. (2023). An Assessment of the Impact of the Mining Industry on Soil and Plant Contamination by Potentially Toxic Elements in Boreal Forests. *Forests, 14,* Article 1641. https://doi.org/10.3390/f14081641

Gupta, S., Jena, V., Matić, N., Kapralova, V., & Solanki, J. S. (2014). Assessment of Geo-Accumulation Index of Heavy Metal and Source of Contamination by Multivariate Factor Analysis. *International Journal of Hazardous Materials, 2,* 18-22.

Hakanson, L. (1980). An Ecological Risk Index for Aquatic Pollution Control. A Sedimentological Approach. *Water Research, 14,* 975-1001.

https://doi.org/10.1016/0043-1354(80)90143-8

Hamid, E., Payandeh, K., Karimi Nezhad, M. T., & Saadati, N. (2022). Potential Ecological Risk Assessment of Heavy Metals (Trace Elements) in Coastal Soils of Southwest Iran. *Frontiers in Public Health, 10,* Article 889130. https://doi.org/10.3389/fpubh.2022.889130

Jahan, I., Reza, A. H. M. S., Haque, M. M., Reza, M. S., & Hasan, M. I. (2024). Soil Pollution and Elemental Sources along Barapukuria Coal Mine, Bangladesh: Implications for Eco-Environmental and Health Risk Assessment. *Heliyon, 10,* e32620. https://doi.org/10.1016/j.heliyon.2024.e32620

Kaiser, H. F. (1974). An Index of Factorial Simplicity. *Psychometrika, 39,* 31-36. https://doi.org/10.1007/bf02291575

Kalnicky, D. J., & Singhvi, R. (2001). Field Portable XRF Analysis of Environmental Samples. *Journal of Hazardous Materials, 83,* 93-122. https://doi.org/10.1016/s0304-3894(00)00330-7

Kazapoe, R. W., Amuah, E. E. Y., & Dankwa, P. (2022). Sources and Pollution Assessment of Trace Elements in Soils of Some Selected Mining Areas of Southwestern Ghana. *Environmental Technology & Innovation, 26,* Article 102329. https://doi.org/10.1016/j.eti.2022.102329

Khalili, R., Zali, A., & Motaghi, H. (2020). Evaluating the Heavy Metals in the Water and Sediments of Haraz River, Using Pollution Load Index (PLI) and Geo Accumulation Index (IGEO). *Iranian Journal of Soil and Water Research, 52,* 933-942.

Liu, D., Wang, J., Yu, H., Gao, H., & Xu, W. (2021). Evaluating Ecological Risks and Tracking Potential Factors Influencing Heavy Metals in Sediments in an Urban River. *Environmental Sciences Europe, 33,* Article No. 42. https://doi.org/10.1186/s12302-021-00487-x

Luo, X., Ren, B., Hursthouse, A. S., Jiang, F., Deng, R., & Wang, Z. (2021). Source Identification and Risk Analysis of Potentially Toxic Elements (PTEs) in Rainwater Runoff from a Manganese Mine (South Central Hunan, China). *Water Supply, 21,* 824-835. https://doi.org/10.2166/ws.2020.352

Mahvi, A. H., Eslami, F., Baghani, A. N., Khanjani, N., Yaghmaeian, K., & Mansoorian, H. J. (2022). Heavy Metal Pollution Status in Soil for Different Land Activities by Contamination Indices and Ecological Risk Assessment. *International Journal of Environmental Science and Technology, 19,* 7599-7616. https://doi.org/10.1007/s13762-022-03960-z

Mensah, A. K., Sekyi-Annan, E., & Amoakwah, E. (2025). Availability and Mobilisation of Potentially Harmful Elements in Contaminated Mining Sites: A Systematic Review of Using Soil Amendments and Plants for Remediation. *Journal of Trace Elements and Minerals, 12,* Article 100234. https://doi.org/10.1016/j.jtemin.2025.100234

Müller, G. (1969). Index of Geoaccumulation in Sediments of the Rhine River. *GeoJournal, 2,* 108-118.

NIST (2009). *Certificate of Analysis: Standard Reference Material 2711a, Montana II Soil.* NIST.

Oberthür, T., Weiser, T., Amanor, J. A., & Chryssoulis, S. L. (1997). Mineralogical Siting and Distribution of Gold in Quartz Veins and Sulfide Ores of the Ashanti Mine and Other Deposits in the Ashanti Belt of Ghana: Genetic Implications. *Mineralium Deposita, 32,* 2-15. https://doi.org/10.1007/s001260050068

Odling, A. (2022). *Stress-Transfer Modelling of Gold Systems at the Obuasi Gold Deposit, Ghana* (pp. 16-19). Doctoral Dissertation, Cardiff University.

Oliver, N. H. S., Allibone, A., Nugus, M. J., Vargas, C., Jongens, R., Peattie, R. et al. (2020). Chapter 6: The Supergiant, High-Grade, Paleoproterozoic Metasedimentary Rock- and Shear Vein-Hosted Obuasi (Ashanti) Gold Deposit, Ghana, West Africa. In S. F. Simmons,

B. M. Tutolo, S. L. L. Barker, R. J. Goldfarb, & R. Francois (Eds.), *Geology of the World's Major Gold Deposits and Provinces* (pp. 121-140). Society of Economic Geologists. https://doi.org/10.5382/sp.23.06

Olympus Corporation (n.d.) *Vanta VMR Geochemistry LOD*. Olympus Corporation.

Rizvi, N. B., Sarwar, A., Waheed, S., Iqbal, Z. F., Imran, M., Javaid, A. et al. (2024). Nano-Based Remediation Strategies for Micro and Nanoplastic Pollution. *Journal of Contaminant Hydrology, 265,* Article 104380. https://doi.org/10.1016/j.jconhyd.2024.104380

Selahvarzi, M., Sobhanardakani, S., Hemmasi, A. H., Taghavi, L., & Ghoddousi, J. (2023). Contamination and Source Apportionment of Iron, Zinc, Cadmium and Chromium Elements in Surface Soil of Khorramabad County, Iran. *Iranian Journal of Health and Environment, 15,* 651-670.

Sunkari, E. D., Appiah-Twum, M., & Lermi, A. (2019). Spatial Distribution and Trace Element Geochemistry of Laterites in Kunche Area: Implication for Gold Exploration Targets in NW, Ghana. *Journal of African Earth Sciences, 158,* Article 103519. https://doi.org/10.1016/j.jafrearsci.2019.103519

Sunkari, E. D., Oppong, O., & Agbenyezi, T. K. (2024). Petrogenetic and Geochemical Characteristics of Some Auriferous Granitoids in the Kumasi Basin, Ghana: Implications for Geodynamic Settings and Controls of Orogenic Gold Mineralization in the Edikan Gold Mine. *Deep Underground Science and Engineering, 4,* 406-421. https://doi.org/10.1002/dug2.12128

Sutherland, R. A. (2000). Bed Sediment-Associated Trace Metals in an Urban Stream, Oahu, Hawaii. *Environmental Geology, 39,* 611-627. https://doi.org/10.1007/s002540050473

Tomlinson, D. L., Wilson, J. G., Harris, C. R., & Jeffrey, D. W. (1980). Problems in the Assessment of Heavy-Metal Levels in Estuaries and the Formation of a Pollution Index. *Helgoländer Meeresuntersuchungen, 33,* 566-575. https://doi.org/10.1007/bf02414780

Turekian, K. K., & Wedepohl, K. H. (1961). Distribution of the Elements in Some Major Units of the Earth's Crust. *Geological Society of America Bulletin, 72,* 175-192. https://doi.org/10.1130/0016-7606(1961)72[175:doteis]2.0.co;2

USEPA (2007). *Method 6200: Field Portable X-Ray Fluorescence Spectrometry for the Determination of Elemental Concentrations in Soil and Sediment*. USEPA.

Xiao, L., Zhou, Y., Huang, H., Liu, Y., Li, K., Li, M. et al. (2020). Application of Geostatistical Analysis and Random Forest for Source Analysis and Human Health Risk Assessment of Potentially Toxic Elements (PTEs) in Arable Land Soil. *International Journal of Environmental Research and Public Health, 17,* Article 9296. https://doi.org/10.3390/ijerph17249296

Zhang, B., Hou, H., Huang, Z., & Zhao, L. (2023a). Estimation of Heavy Metal Soil Contamination Distribution, Hazard Probability, and Population at Risk by Machine Learning Prediction Modeling in Guangxi, China. *Environmental Pollution, 330,* Article 121607. https://doi.org/10.1016/j.envpol.2023.121607

Zhang, Y., Lei, M., Li, K., & Ju, T. (2023b). Spatial Prediction of Soil Contamination Based on Machine Learning: A Review. *Frontiers of Environmental Science & Engineering, 17,* Article 93. https://doi.org/10.1007/s11783-023-1693-1